Single-Event and Total Dose Testing for Advanced Electronics

Jonathan Pellish
NASA Goddard Space Flight Center

Table of Contents

Acknowledgements

I have lots of people to acknowledge after being given the opportunity to present a short course section at the 2012 Institute of Electrical and Electronics Engineers (IEEE) Nuclear and Space Radiation Effects Conference (NSREC). I would like thank my colleagues at Vanderbilt University, especially Dr. Ron Schrimpf, this year's short course chairman. I also extend thanks to Mr. Ken LaBel, the NASA Goddard Space Flight Center's Radiation Effects and Analysis Group, the NASA Electronic Parts and Packaging program, and the Defense Threat Reduction Agency's Radiation Hardened Microelectronics Program for supporting the development of this short course. Thanks also go the many technical reviewers whose insights and commentary have made a positive impact.

Acronyms

amu	Atomic Mass Unit
ASIC	Application-Specific Integrated Circuit
ASTM	American Society for Testing and Materials
AU	Astronomical Unit
BEOL	Back-End-Of-Line
CGS	Centimeter–Gram–Second (system of units)
CME	Coronal Mass Ejection
CMOS	Complementary Metal Oxide Semiconductor
COTS	Commercial-Off-the-Shelf
DDD	Displacement Damage Dose
DDR	Double Data Rate (SDRAM)
ELDRS	Enhanced Low-Dose-Rate Sensitivity
ESP	Emission of Solar Protons
FET	Field Effect Transistor
FPGA	Field Programmable Gate Array
GCR	Galactic Cosmic Rays
GEO	Geostationary Orbit (sometimes interchanged with geosynchronous)
GeV	Giga-electron Volt
HBT	Heterojunction Bipolar Transistor
IEEE	Institute of Electrical and Electronics Engineers
IRPP	Integral Rectangular Parallelepiped
ISO	International Organization for Standardization
ITRS	International Technology Roadmap for Semiconductors
keV	Kilo-electron Volt
LEO	Low-Earth Orbit
LET	Linear Energy Transfer
MBU	Multiple-Bit Upset
MEO	Medium-Earth Orbit
MeV	Mega-electron Volt
MOSFET	Metal Oxide Semiconductor Field Effect Transistor

NSREC	Nuclear and Space Radiation Effects Conference
PSYCHIC	Prediction of Solar particle Yields for CHaracterizing Integrated Circuits
RHA	Radiation Hardness Assurance
RHBD	Radiation-Hardened (Hardening) by Design
RHBP	Radiation-Hardened (Hardening) by Process
RPP	Rectangular Parallelepiped
SDRAM	Synchronous Dynamic Random Access Memory
SEB	Single-Event Burnout
SEE	Single-Event Effects
SEFI	Single-Event Functional Interrupt
SEGR	Single-Event Gate Rupture
SEL	Single-Event Latchup
SET	Single-Event Transient
SEU	Single-Event Upset
SI	International System of Units (*Système international d'unités*)
SOI	Silicon-On-Insulator
SRAM	Static Random Access Memory
SWaP	Size, Weight, and Power
TID	Total Ionizing Dose

1 Introduction

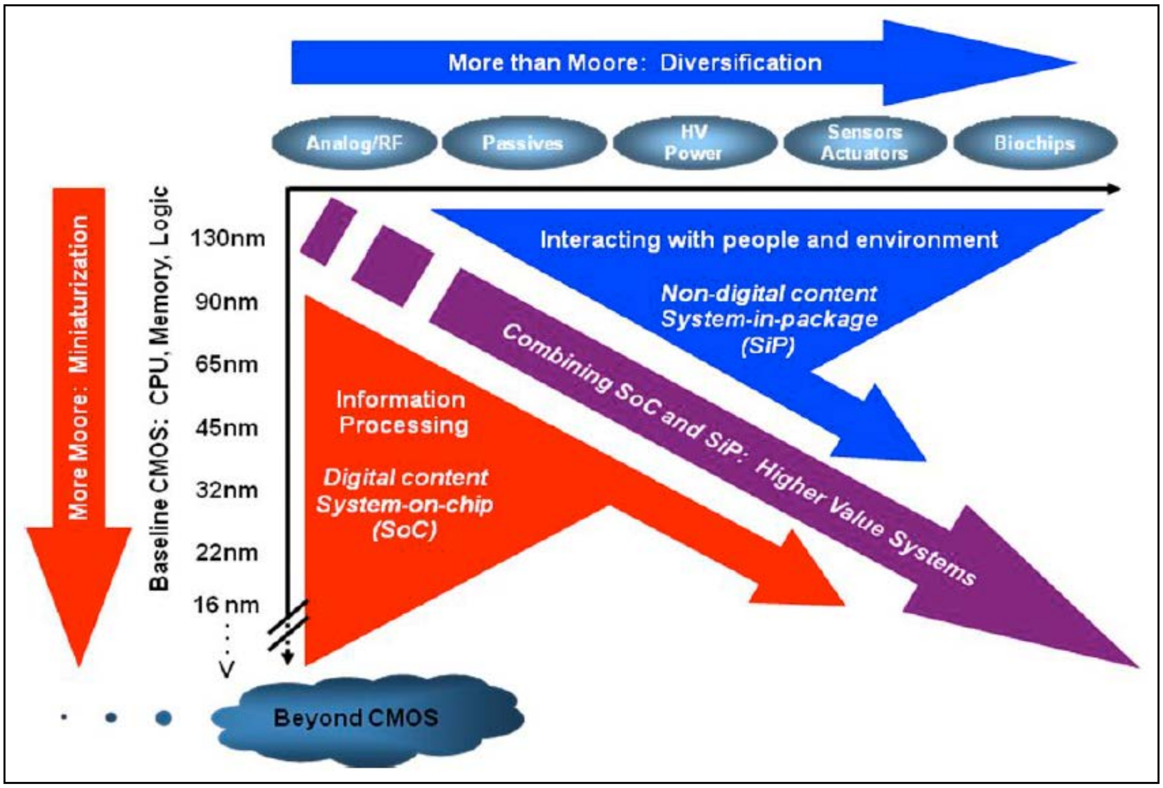

Figure 1: Moore's Law and More [1]

Advanced electronics are relative to each generation of practitioners in the field of radiation effects for aerospace electronic systems. There has been a steady progression of technology scaling over the past four decades, mostly related to CMOS process technologies in recent years. Companies scale process technologies to reduce cost per unit due to economy of scale and to increase performance via smaller transistors and higher transistor densities per unit area. However, this scaling has come at enormous costs related to manufacturing complexity and power density.

Many people may assume that "advanced electronics" refers to CMOS ASICs, but the scope of this short course will interpret the term more broadly. The term "advanced" means the electronic devices in question improve the tradespace of size, weight, and power for the intended system application. For convenience, "size, weight, and power" are often denoted as SWaP in these types of system applications. SWaP improvements could be related to a new type of data converter, microprocessor, SRAM, NAND flash non-volatile memory, operational amplifier, SDRAM, or power MOSFET. These devices are not necessarily fabricated in the latest CMOS process, but they nevertheless are considered advanced electronics because of the benefits they provide at the system level. Figure 1 shows some advanced technology examples from the 2011 ITRS, both those related to continuous technology scaling and those related to extending existing technologies via increased integration [1]. What was once advanced technology is now commonplace. As the world's technology leaders continue to scale microelectronics, the array of different technologies and devices will increase concurrently with complexity. The radiation effects community will have to meet the evaluation and qualification challenges of these advanced technologies in order to continue evolving the capabilities of our systems in a safe and efficient manner.

More importantly for our community, technology scaling has also affected the radiation response of the latest technologies used for aerospace systems. Scaling affected the mechanisms driving total ionizing dose (TID), displacement damage dose (DDD), and destructive and non-destructive single-event effects (SEE) tolerance. This has precipitated large radiation effects research programs within industry, government, and academia aimed at understanding the effects of scaling on the current state-of-the-practice for radiation effects. We found that many previous constructs and assumptions were still valid, but just as many were broken without easy fixes.

As scaling and process integration continues to progress, the radiation effects community continues to adapt. The behavior of previous technology generations has become a less than ideal indicator of future technologies as evidenced by the many recent investigations on single-event transients (SETs) [2-13], heavy ion indirect ionization [14-18], and low-energy proton effects [19-23][1]. These investigations have resulted in the breakdown of some traditional assumptions pertaining to linear energy transfer (LET) and the rectangular parallelepiped (RPP) and integral RPP (IRPP) rate calculation methods, leading to increased analysis complexity and additional difficulty in bounding on-orbit SEE rate calculations.

This short course will cover an introduction to the natural space radiation environment, space environment impacts on electronic devices, evaluation of total ionizing dose, and

[1] Note that given references are not meant to be exhaustive

evaluation of single-event effects. While certainly relevant to radiation effects, displacement damage dose will not be a primary focus in this short course. We refer the reader to the many good background references on this subject that are published in the radiation effects literature – several examples include [24-26].

2 Advanced Technologies in Space Electronics

2.1 Changing Landscape

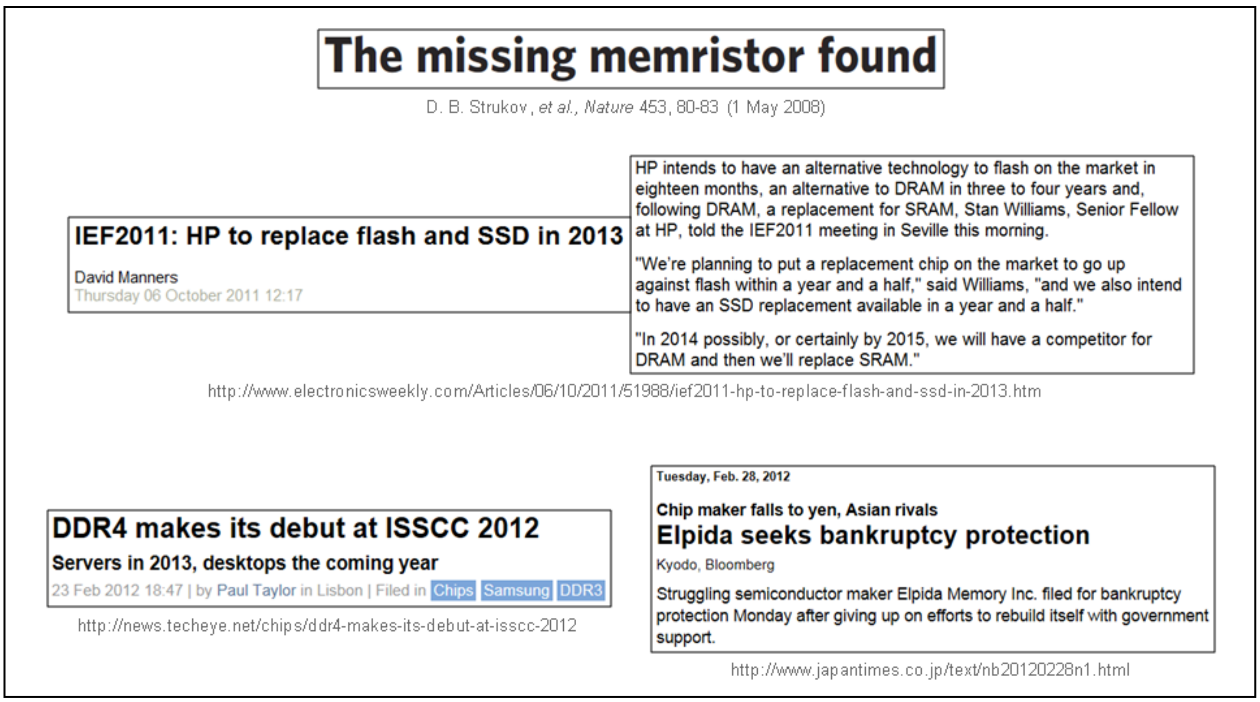

The missing memristor found

D. B. Strukov, *et al., Nature* 453, 80-83 (1 May 2008)

IEF2011: HP to replace flash and SSD in 2013

David Manners
Thursday 06 October 2011 12:17

HP intends to have an alternative technology to flash on the market in eighteen months, an alternative to DRAM in three to four years and, following DRAM, a replacement for SRAM, Stan Williams, Senior Fellow at HP, told the IEF2011 meeting in Seville this morning.

"We're planning to put a replacement chip on the market to go up against flash within a year and a half," said Williams, "and we also intend to have an SSD replacement available in a year and a half."

"In 2014 possibly, or certainly by 2015, we will have a competitor for DRAM and then we'll replace SRAM."

http://www.electronicsweekly.com/Articles/06/10/2011/51988/ief2011-hp-to-replace-flash-and-ssd-in-2013.htm

DDR4 makes its debut at ISSCC 2012

Servers in 2013, desktops the coming year

23 Feb 2012 18:47 | by Paul Taylor in Lisbon | Filed in Chips Samsung DDR3

http://news.techeye.net/chips/ddr4-makes-its-debut-at-isscc-2012

Tuesday, Feb. 28, 2012

Chip maker falls to yen, Asian rivals

Elpida seeks bankruptcy protection

Kyodo, Bloomberg

Struggling semiconductor maker Elpida Memory Inc. filed for bankruptcy protection Monday after giving up on efforts to rebuild itself with government support.

http://www.japantimes.co.jp/text/nb20120228n1.html

Figure 2: Several recent technology turnover/change examples from the news. The references from top-to-bottom are [27-30].

The commercial electronics community moves quickly, releasing new technologies and products at a rapid pace with examples of this shown in Figure 2. Many groups in the aerospace community would like to implement systems using advanced technologies, but the time required to screen and qualify new components makes them practically obsolete by the time they are ready to fly. SDRAMs are a great example of this, where many groups are grappling with the issues of testing DDR2 and DDR3 devices when DDR4 has already been announced [29]. The same can also be said for ASICs, which can benefit from fabrication in scaled CMOS processes.

Table 1: Examples of Progression in Spaceflight Memories and Radiation Testing Considerations

THEN	NOW
Magnetic core memory	NAND flash, resistive random access memory (RAM), magnetic RAM, phase-change RAM, programmable metallization cell RAM, and double-data rate (DDR) synchronous dynamic RAM (SDRAM)
Single-bit upset (SBU) and single-event transients (SETs)	Multiple-bit upset (MBU), block errors, single-event functional interrupts (SEFIs), frequency-dependence
Heavy ions and high-energy protons	Heavy ions, high- and low-energy protons, and delta rays
Radiation hardness assurance (RHA)	RHA what?

Table 1 gives a few relevant examples of the historical progression in spaceflight memory devices and radiation testing considerations. While we will not address development of spaceflight memories, they have been key fixtures in the radiation effects evaluation of new technologies. The common theme in Table 1 is a progression from less complex and well-defined to more complex and less-defined. We address this general theme as well as what it means for radiation hardness assurance (RHA) and believe it is at the root of radiation effects evaluation when considering advanced technologies.

It is important to define what we mean by RHA so that we can differentiate it from engineering characterization or evaluation. In our case it is the methods used to assure that microelectronic components meet specified requirements for *system operation* at specified *radiation levels* for a given *probability of survival* and level of *confidence* – after [31]. Radiation evaluation, as opposed to RHA, does not necessarily have an identified system or a target radiation environment. Regardless, advanced technologies that increase system capabilities also introduce additional evaluation challenges, which affect testability.

2.2 Examples

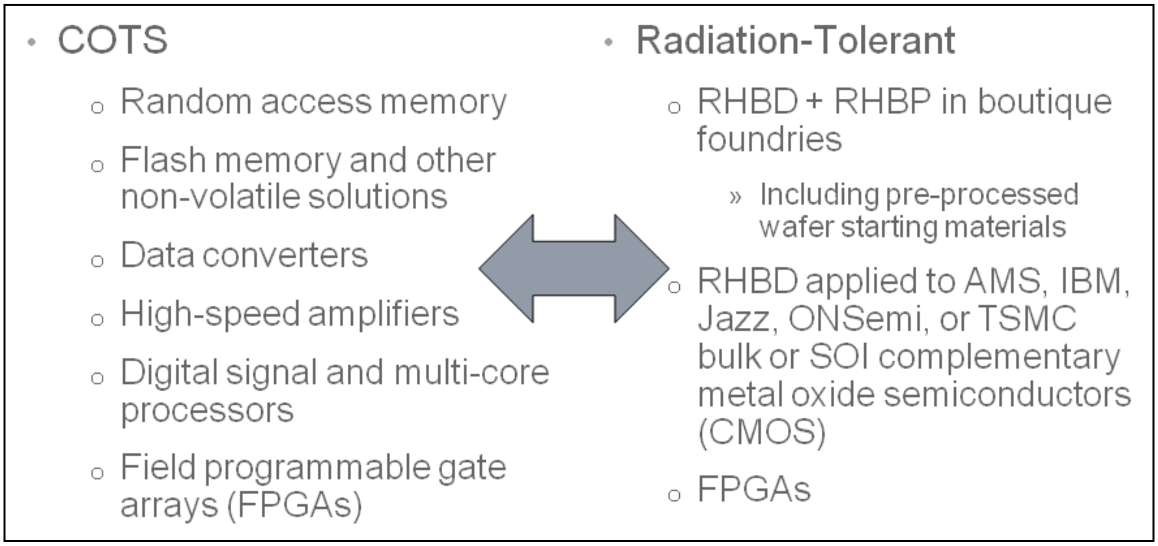

Figure 3: Examples of COTS and radiation tolerant advanced microelectronics that can be used in various spaceflight systems. AMS, formerly AustriaMicroSystems; TSMC, Taiwan Semiconductor Manufacturing Co.; SOI, silicon-on-insulator.

There are two general types of advanced electronic technologies used in space: commercial-off-the-shelf (COTS) and radiation tolerant [32]. COTS electronics are designed with no attempt to mitigate radiation effects. COTS can refer to commodity devices or to ASICs designed using a commercially-available design system. Radiation tolerant electronics are designed explicitly to account for and mitigate radiation effects by process and/or design. Some examples of these device types are shown in Figure 3, and include memories, data converters, microprocessors, and FPGAs. These types of devices can also be implemented using radiation hardened by design (RHBD) and radiation hardened by process (RHBP) techniques to achieve tolerance or immunity to both total ionizing dose and single-event effects. Often, many radiation tolerant electronic components use both RHBD and RHBP methods to achieve the desired level of performance. An example of this might be a SRAM that uses both RC feedback and an epitaxial layer in the substrate to mitigate multiple types of SEE.

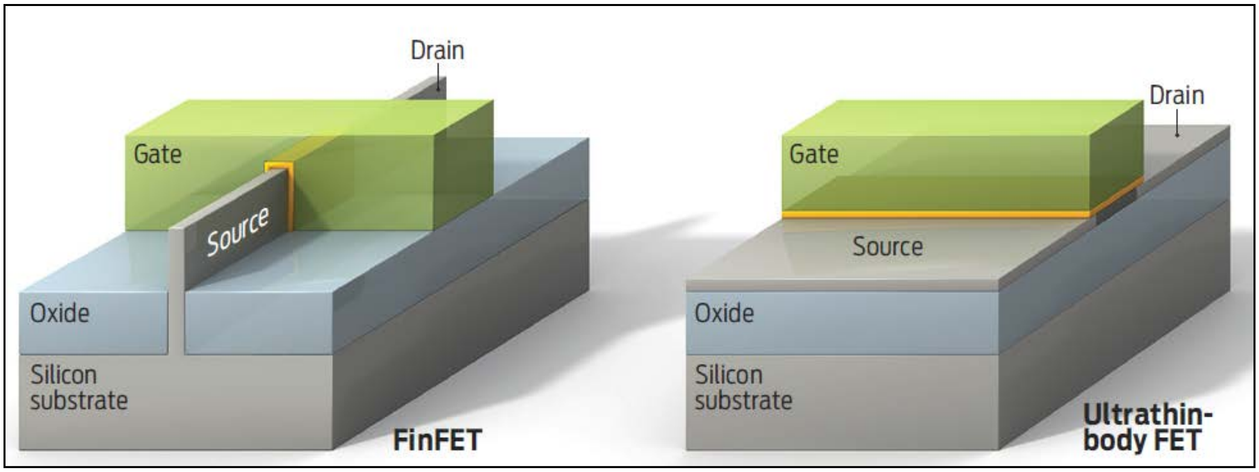

Figure 4: *IEEE Spectrum* article from 2011 that describes the recently-released Intel Corp. tri-gate 3-D FET (shown on left) [33]. These 3-D transistors are built into Intel's 22 nm Ivy Bridge microprocessor. As a point of clarification, the Intel FinFETs are more accurately characterized as tri-gate devices since there are three conducting channel faces.

The discrete components listed in Figure 3 are complimented by advanced process technologies. Intel Corp. announced the most significant news in this area recently, when they disclosed that their 22 nm bulk CMOS process included tri-gate, 3-dimensional (3-D) FETs. This type of device is shown in Figure 4, where it is compared with a planar, ultrathin-body FET. While research-grade 3-D transistors have existed for some time, Intel is the first company to mass produce them in a commercial product. Other advanced CMOS fabrication processes are available from companies like IBM Corp. and Taiwan Semiconductor Manufacturing Co.

While CMOS processes tend to dominate the advanced technology scene, there are several other process technologies – like SiGe BiCMOS, GaAs, and GaN – that present additional options as well as evaluation challenges. Of these, it is fair to say that SiGe-based technologies have received the most attention in the radiation literature over the past decade or so. Companies like IBM, Jazz Semiconductor, Texas Instruments, and IHP all use SiGe to produce heterojunction bipolar transistors (HBTs), which are typically integrated with standard CMOS process flows. This makes an ideal platform for mixed-signal, high-speed data, and radio frequency applications. For more information on SiGe BiCMOS technologies and their radiation response characteristics, we refer the reader to other articles [34-40].

3 Natural Space Radiation Environment

3.1 Particle Sources and Solar Cycle Modulation

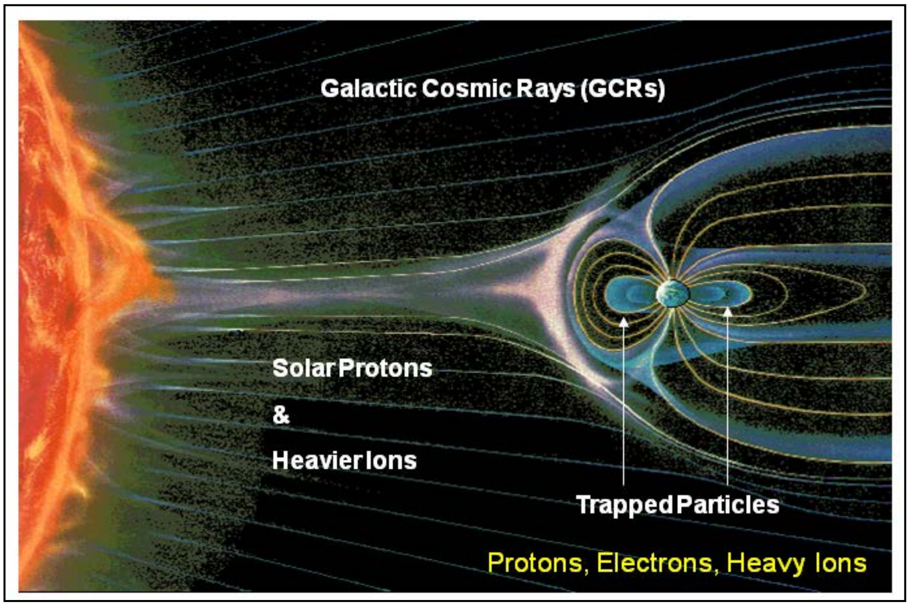

Figure 5: Artist's depiction of the natural space radiation environment local to the Earth, after K. Endo, Nikkei Science Inc. of Japan and J. L. Barth [41]. It is composed of solar particles, particles trapped in the Earth's magnetic field, and galactic cosmic rays (GCR). These particles include electrons, protons, and every naturally-occurring element in the periodic table. These particle environments can be very dynamic and are modulated by the solar cycle.

Spacecraft must endure a number of environmental hazards, including high-energy particle radiation, x-ray and ultraviolet radiation, and low-energy plasma. We will focus specifically on the high-energy particles, since those are the kind most likely to affect advanced electronics in the space environment. We will not consider man-made radiation environments. There are three general categories of high-energy particles found in the natural space radiation environment: 1) the background flux[2] of ions that originates outside our solar system, called galactic cosmic rays (GCR); 2) particles that are emitted from the Sun during solar particle events like solar flares and coronal mass ejections (CMEs); and, 3) those particles trapped by planetary magnetic fields like the Earth's Van Allen Belts. These particle environments are shown in the artist's rendering in Figure 5. Solar activity modulates GCR fluxes and the frequency of solar particle events,

[2] Flux is defined as the number of particles or photons per unit time and often contains differential elements for energy and solid angle. Typical differential units for ions like GCR are particles/(m^2-s-sr-(MeV/amu)).

making that portion of the space environment very dynamic at times. The space environment's dynamic behavior complicates environmental predictions for spaceflight missions and is one of the primary reasons that design margin is a necessity. We will cover a top-level description of the space environment, but cannot hope to give a complete description. For additional short course material on the space environment, there are several other short courses on the subject [41-43].

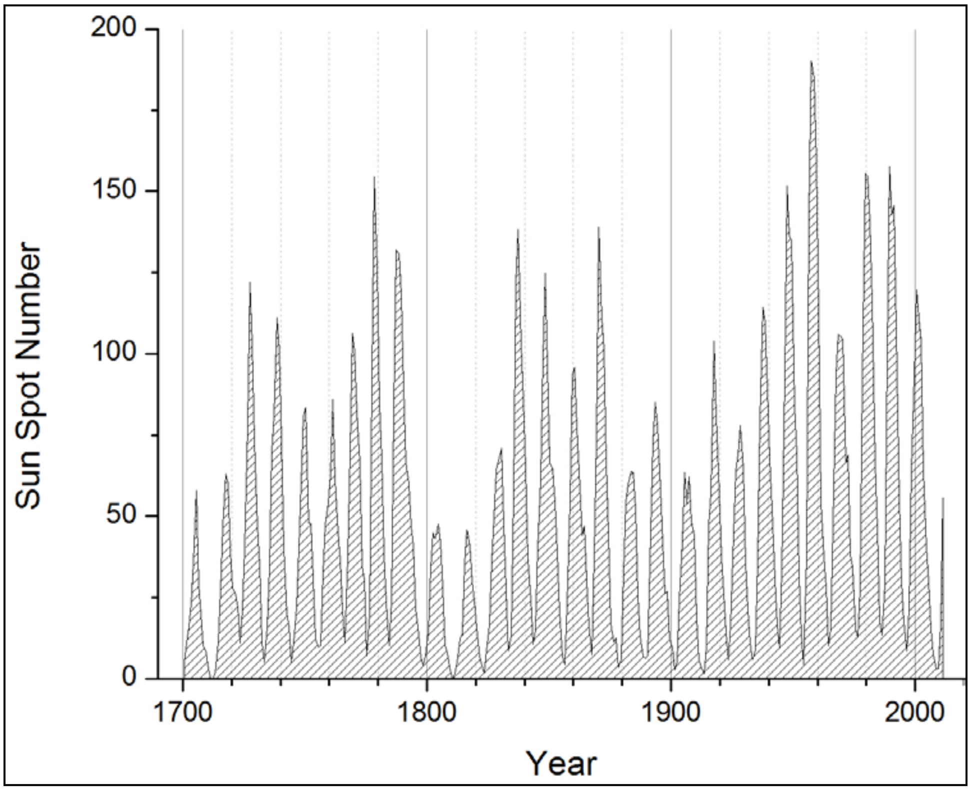

Figure 6: These sun spot data were downloaded from the Solar Influences Data Analysis Center, which is publically available at http://sidc.oma.be/index.php/. There are similar data available via the National Weather Service's Space Weather Prediction Center, located at http://www.swpc.noaa.gov/. Note the 11-year solar cycle with solar maximum indicated by large numbers of sun spots.

The Sun serves as both a producer and modulator of particles in the space environment. As shown in Figure 6, solar modulation is cyclical with a primary period of approximately 11 years. During the 11-year cycle, there are approximately 4 years when solar activity levels are low, called solar minimum, and 7 years when activity is elevated, called solar maximum. The 7 active years are assumed to span a starting point 2.5 years before and an ending point 4.5 years after a time defined by the maximum sunspot number in the cycle [44]. For the past several solar cycles, the maximum sun spot number occurred at 1968.9, 1979.9, 1989.6, and 2000.2 – cycle 24 is projected to peak at 2013.4. At the end of each 11-year period the magnetic polarity of the Sun reverses, so there is a larger 22-year cycle. However, the magnetic polarity only appears to affect GCR fluxes and not trapped particle populations or solar particle event fluxes [45]. Because of the limited effect of the Sun's magnetic polarity, solar modulation is usually based on an 11-year cycle.

3.2 Particle Abundances and Energy Ranges

3.2.1 Galactic Cosmic Rays

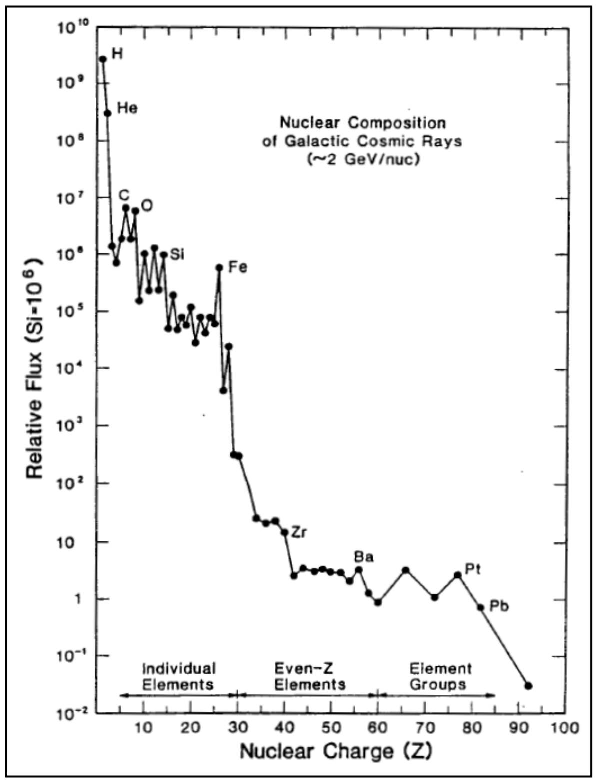

(a)

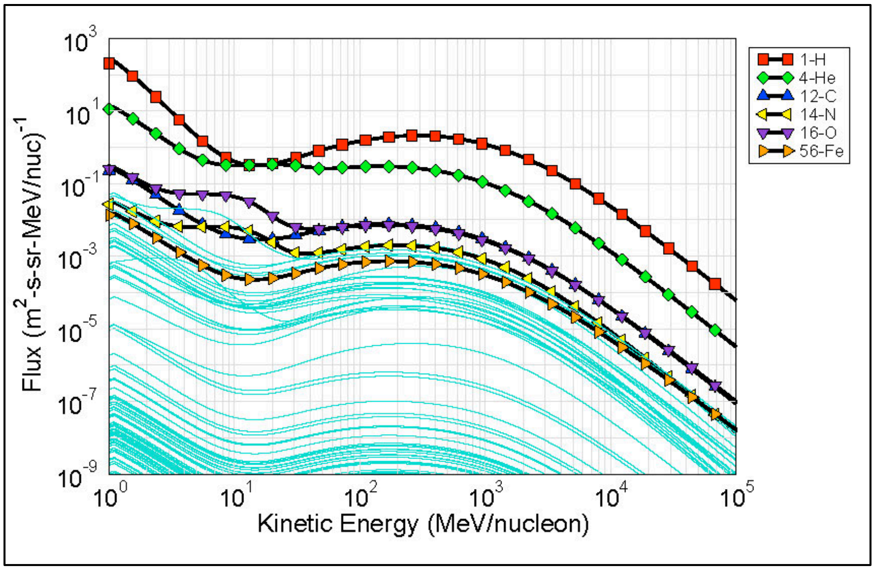

(b)

Figure 7: (a) GCR relative abundances by nuclear charge (*Z*), normalized to Si = 1000 for *Z* < 28 and Si = 10^6 for *Z* ≥ 29 [46]; and, (b) differential flux of GCR as predicted by the Moscow State University model implemented in the CREME96 tool [47, 48] and available on the CREME-MC website https://creme.isde.vanderbilt.edu/ – the six primary elements are shown in the legend. Note the large GCR energy range and the fact that the high-energy flux peak is several hundred MeV/amu to around 1 GeV/amu.

GCR originate outside the solar system, possibly accelerated by supernovae, and permeate the universe. GCR include all the naturally-occurring elements in the periodic table and are the most energetic of all space radiation. Figure 7 shows the GCR relative abundance and the modeled differential flux as a function of kinetic energy. These charts highlight two trends: GCR abundance drops off rapidly for ions heavier than iron (*Z* = 26), and the primary elements in the environment are H, He, C, N, O, and Fe. Energies of these particles peak around 1 GeV/amu and can be higher than 10^{10} GeV in total kinetic energy. Fluxes for protons and the more abundant ion species are several $cm^{-2} \cdot s^{-1}$ and vary with the solar cycle. Ions with less than 10 GeV/amu of kinetic energy are modulated by the Sun's magnetic field and the solar wind. The greatest GCR flux suppression occurs during solar maximum. We note that there are several GCR models available to practitioners in the radiation effects community. Both Moscow State University (MSU) and NASA have published GCR models [45, 47, 49, 50] and there is also an ISO standard (ISO 15390:2004) based on the MSU models.

3.2.2 Solar Particle Events

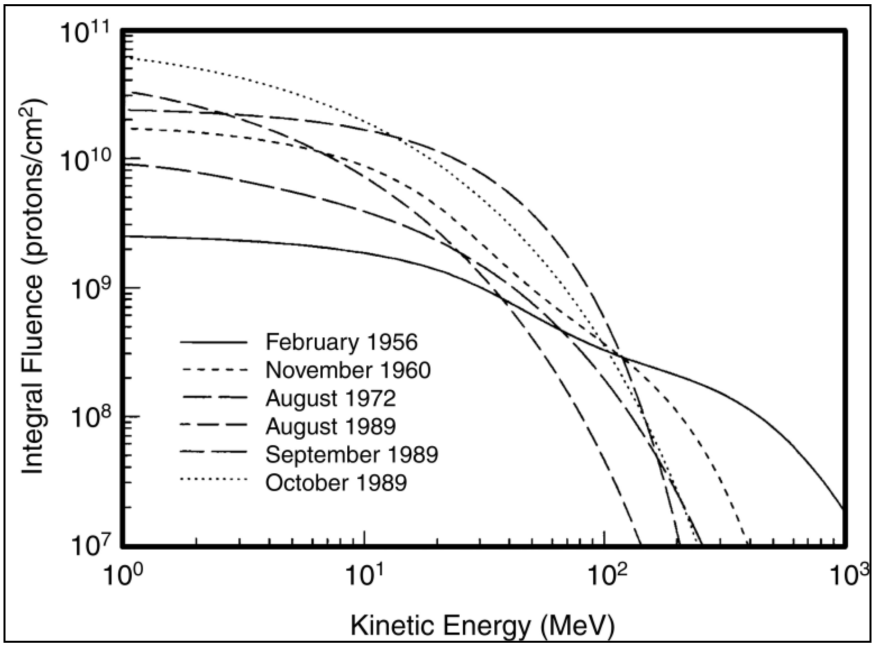

Figure 8: Large solar proton event integral fluence[3] spectra at 1 AU [51]. The August 1972 event dominates in the range of 70-100 MeV. In additional to the importance of the spectral content the August 1972 event, the dominant portion of the exposure occurred over several hours compared to three days of the October 1989 event.

The Sun produces two types of solar particle events: coronal mass ejections (CMEs) and solar flares. As described by M. A. Xapsos in his 2006 NSREC short course [42], solar flares result when the localized energy storage in the coronal magnetic field becomes too great and causes a burst of energy to be released. They tend to be electron rich, last for hours, and have high ^{3}He content relative to ^{4}He. A CME, on the other hand, is a large eruption of plasma (a gas of free ions and electrons) that drives a shock wave outward and accelerates particles. CMEs tend to be proton rich, last for days, and have small ^{3}He content relative to ^{4}He. Some samples of these types of events from solar cycles 20 through 22 are shown through their representative proton fluence spectra in Figure 8. Additional solar particle event spectra can be found in [52, 53]. Two of the larger events shown in Figure 8, "August 1972" and "October 1989," produced

---

[3] Fluence is the integral of flux over a given time interval – *e.g.*, one hour, one year, *etc*. When we refer to the omnidirectional fluence, we will normally mean the "omnidirectional integral (in energy) fluence." The units of this quantity are particles/cm^2.

very high fluxes of protons and heavy ions that would be very damaging to spacecraft electronics…and humans.

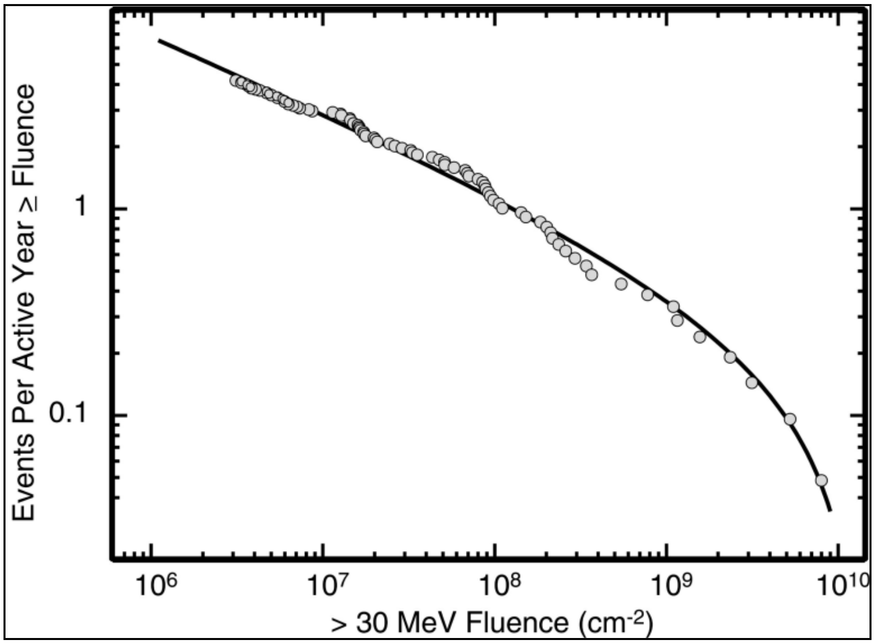

Figure 9: Comparison of the distribution of > 30 MeV solar proton event fluences predicted by the Emission of Solar Protons (ESP) model as compared to data from solar cycles 20 through 22 [54, 55]. An "active year" is defined as per J. Feynman's description – the 7-year period, 2.5 years before and 4.5 years after the peak sunspot number during an 11-year cycle [44].

Due to their stochastic nature, it is difficult to define the content and energy distribution of a solar particle event; this is critical for bounding the performance of advanced electronics on orbit though. To overcome this challenge, several probabilistic solar particle event models were created, including the JPL91 [44] and ESP [54, 55] models. The ESP model, demonstrated in Figure 9, relies on the Maximum Entropy Principle developed by E. Jaynes [56] and produces integral and differential solar proton fluences at specified confidence levels. For example, an ESP-computed integral solar proton fluence has a 10% probability of exceeding ***X*** protons/cm^2 during a 3-year mission, which corresponds to a 90% confidence level that this fluence will not be exceeded during the same time period. The Maximum Entropy approach is useful for mission designs because allowing the user to specify confidence levels permits risk tradeoff studies. As an extension of the ESP model, the PSYCHIC model was developed, which describes solar heavy ion fluences based on the ESP solar proton calculations, so the confidence level feature is preserved [57]. The JPL91, ESP, and PSYCHIC solar particle models are available via toolsets like SPENVIS.

3.2.3 Trapped Particle Environments

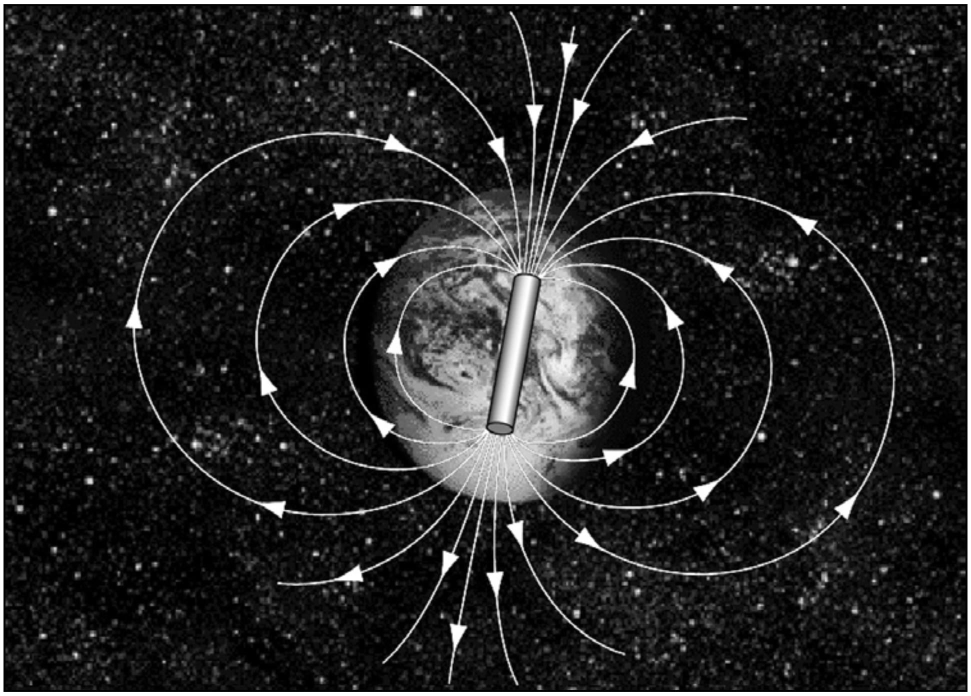

Figure 10: The internal magnetic field of the Earth is approximately a dipole field, which can trap both protons and electrons. Figure after [42].

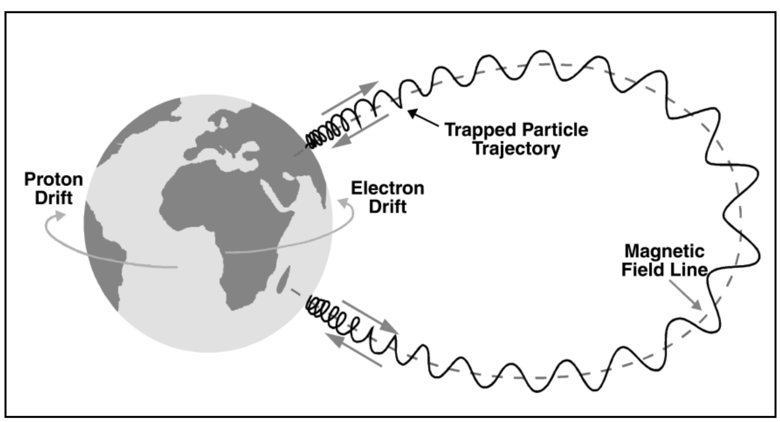

Figure 11: Motion of charged trapped particles in the Earth's magnetic field. After [42] and based on previous work published in [58, 59].

The Earth has both internal and external magnetic fields that make up its magnetosphere. The external field is the result of the solar wind. The internal geomagnetic field originates from within the Earth and is approximately dipolar up to altitudes of about 5 Earth radii; a sketch is shown in Figure 10. This dipole field is tilted about 11° from the Earth's north-south axis and displaced by more than 500 km from the Earth's geocenter [60]. The customary method to describe this dipole field utilizes McIlwain's (*B*,*L*) coordinates, where *L* represents the distance from the origin in the direction of the magnetic equator expressed in Earth radii[4] and *B* is the magnetic field strength [61]. The protons and electrons trapped in these magnetic field lines – called the Van Allen Belts – drift around the Earth and along these field lines forming so-called "drift shells." This motion is shown in Figure 11.

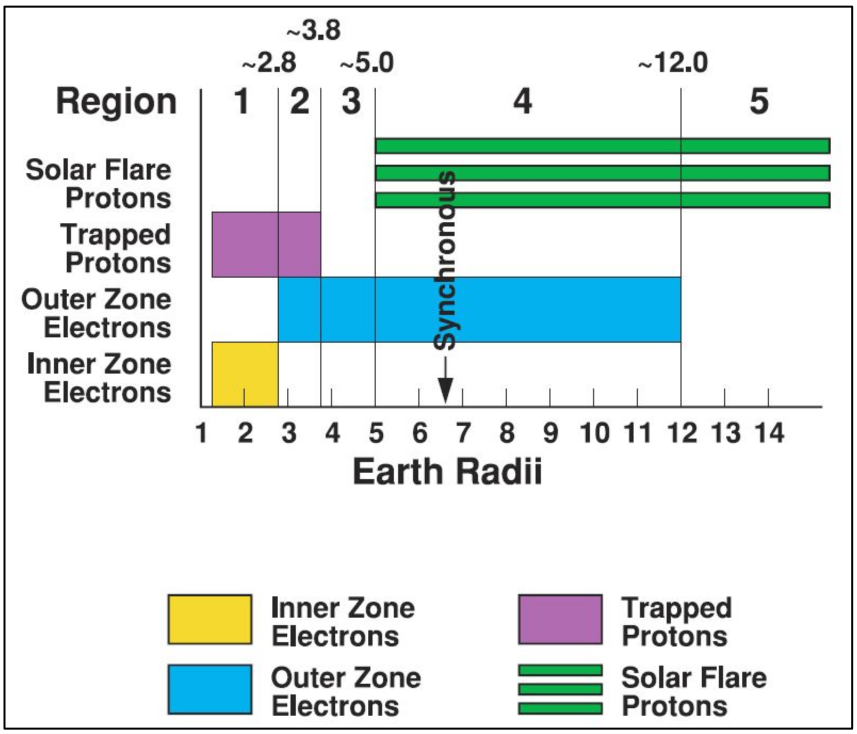

Figure 12: Charged particle distribution in the magnetosphere as a function of Earth radii. This figure was adapted by J. R. Schwank and colleagues after the original published in [59].

[4] For reference, the mean Earth radius is 6371 km. The planet is smaller around the poles and bigger around the equator.

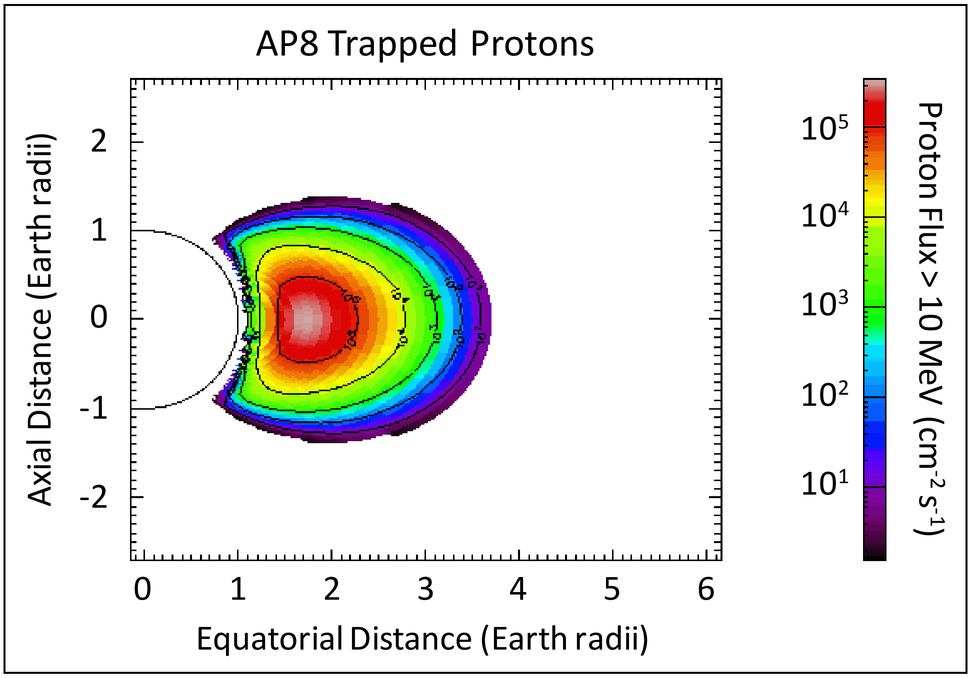

Figure 13: The trapped proton flux population with energies > 10 MeV as predicted by the AP-8 model for solar maximum conditions. The plot was generated using the toolsets available on the SPENVIS website (v4.6.5).

Figure 12 shows charged particle distributions throughout Earth's magnetosphere. We will focus on the trapped protons and electrons since solar protons have already been discussed. Trapped protons have energies up to 100s of MeV, fluxes up to 10^5 $cm^{-2}\cdot s^{-1}$ for energies > 10 MeV, and exist in *L*-shells between 1.15 and 10, though the high-energy protons only exist below altitudes of about 20,000 km. Figure 13 shows a contour plot of AP-8 predicted proton fluxes with energies above 10 MeV, demonstrating that these types of particles are within 4 Earth radii.

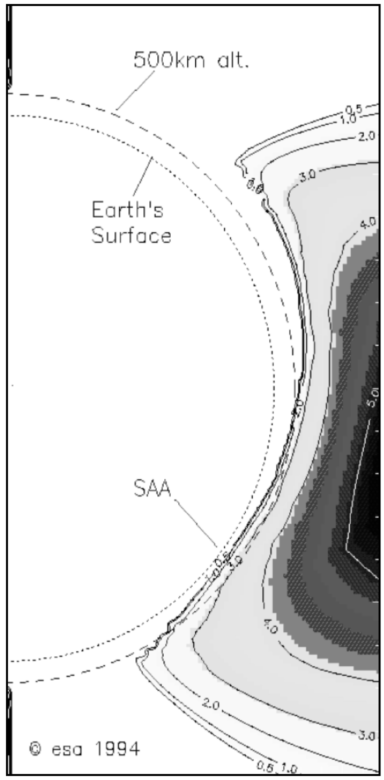

Figure 14: The South Atlantic Anomaly shown as a cut through the Earth at meridian 325° with proton (> 10 MeV) radiation belt fluxes represented by a grey-scale. The Earth's surface and 500 km altitude level are shown. The dipping of the proton belt within the 500 km level in the South Atlantic clearly visible [60].

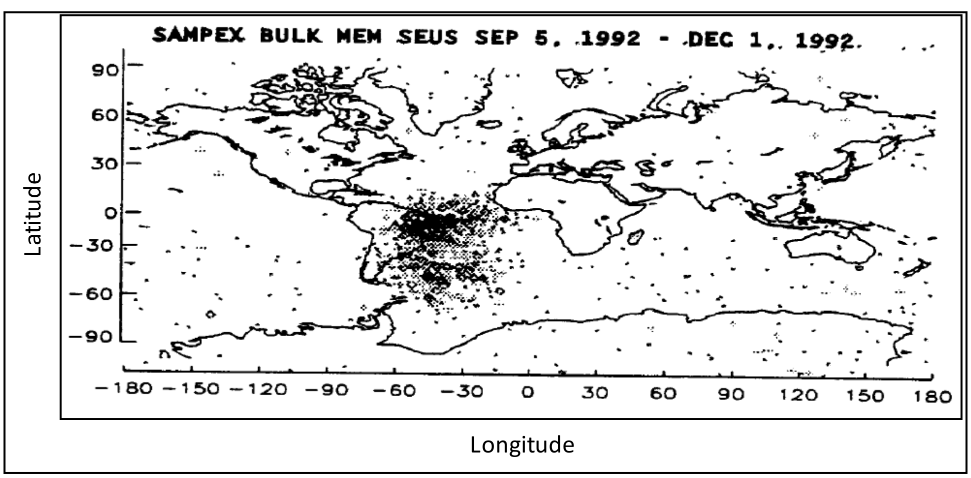

(a)

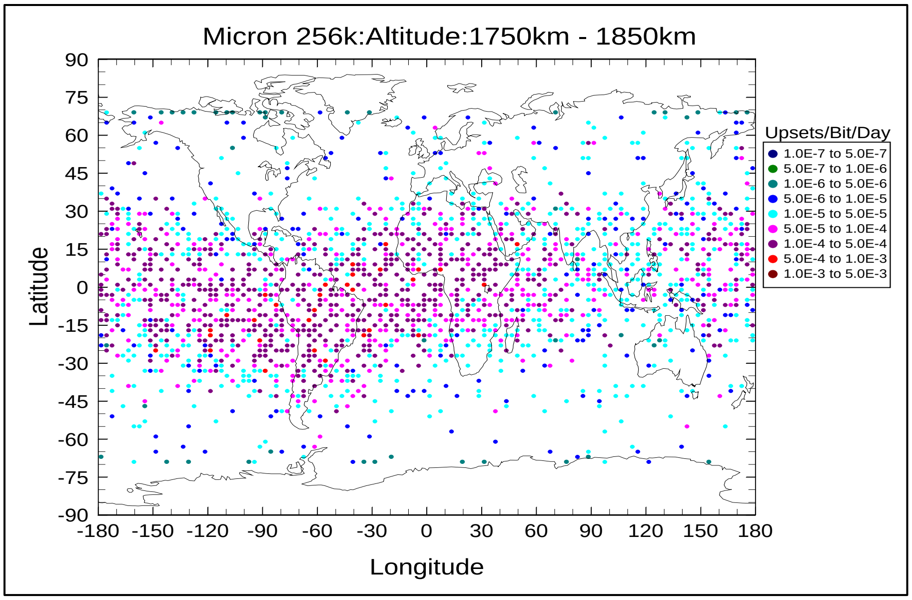

(b)

Figure 15: (a) Solar Anomalous Magnetospheric Explorer (SAMPEX) solid state recorder single-event upsets correlated with the SAA [62]; (b) single-event upsets from memory experiments aboard the Cosmic Ray Upset Experiment (CRUX) Advanced Photovoltaic and Electronics Experiment (APEX) [63]. The SAA and associated proton belts are visible via the recorded data errors in the memories.

The dipole tilt and displacement of the Earth's geomagnetic field relative to its rotation axis produces a phenomenon called the "South Atlantic Anomaly," (SAA) which is a feature of the trapped proton environment that dominates spacecraft orbits below 1000 km. Because of the tilt and displacement, part of the inner edge of the trapped proton belts is at a much lower altitude off the southeast coast of Brazil, which is how the feature received its name. The SAA is shown graphically in Figure 14 and results of volatile memories flying through the SAA and associated trapped proton belts in Figure 15, where the memory data errors provide evidence of the protons' existence.

There are various Earth-based trapped proton models available to interested users, including AP-8 [64], CRRESPRO [65], and one based on SAMPEX/PET data [66]. There are limitations to each of these models, so understanding environment and operational details is important. A broad consortium is currently in the process of updating the legacy AP-8 model to what will become the AP-9 model. There are trapped proton models for other planets, such as the Jovian environment [67], but those will not be covered here.

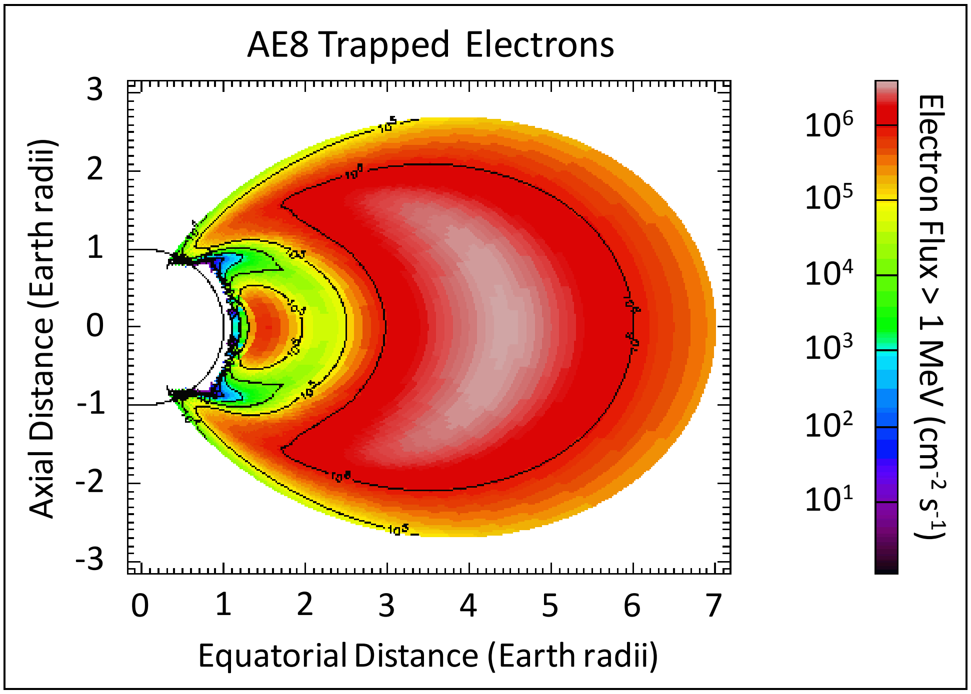

Figure 16: The trapped electron flux population with energies > 1 MeV as predicted by the AE-8 model for solar maximum conditions. The inner and outer electron belts are clearly visible. The plot was generated using the toolsets available on the SPENVIS website (v4.6.5).

Trapped electrons have energies up to 10 MeV, fluxes up to 10^6 cm-2•s-1 for energies > 1 MeV, and exist in two *L*-shell regions, an inner and outer belt – between 1 and 2.8 and between 2.8 and ~10. Figure 16 shows a contour plot of AE-8 predicted electron fluxes with energies above 1 MeV, which clearly shows the two trapped electron zones. As with protons, there are several available trapped electron models for Earth, including AE-8 [68], CRRESELE [69], and IGE-2006/POLE [70-72]. For additional references on trapped environments for other planets, such as the Jovian system, see [67].

3.2.4 Spacecraft Trajectories and Summary of Radiation Environment Threats

The following tables are meant as reference points and to summarize typical spacecraft trajectories by listing the associated natural space radiation environment hazards. All spacecraft trajectories include some portion of the space radiation environment. The severity of the radiation environment in each of these orbits is proportional to the time spent in the trapped radiation environments and cumulative exposure to solar particle events. It is important to note the substantial radiation environment difference between an equatorial and polar LEO trajectory.

Table 2: Common Spacecraft Trajectories

Name	Location	Uses	Examples
LEO (Low-Earth Orbit)	< 3,000 km (most < 900 km)	All applications (cheapest to get to)	Space telescope, ISS, LandSat, Iridium
MEO (Medium-Earth Orbit)	3,000 km to GEO	Communications, navigation, some observation	GPS
HEO (Highly Elliptical Orbit) [also called Molniya Orbits]	Typically perigee in LEO and apogee near GEO	Communications	Communication satellites
GEO (Geosynchronous)	35,856 km	Communications, weather	TDRS, Intelsat, DBS (radio, TV), GOES
Super-Synchronous	Above GEO, below the Moon	Limited	Vela
Lunar and Lagrange Point	At or near Moon distance (350,000 km)	Science, potentially manufacturing	Apollo, Lunar orbiters, SOHO, WMAP
Interplanetary, Deep Space	Beyond the Moon, within the solar system	Exploration	Viking, Mars Pathfinder, Galileo, Mars Rovers
Interstellar	Outside the solar system	Exploration	Pioneer 10, 11

*After Table 9-7 in [73]

Table 3: Radiation Threat Summary for the Trajectories in Table 2

Name	Trapped Electrons	Trapped Protons	Solar Particles	Cosmic Rays
LEO Low-Inclination	Moderate	Yes	No	Moderate
LEO Polar	Moderate	Yes	Yes	Yes
MEO	Severe	Severe	Yes	Yes
HEO	Yes	Yes	Yes	Yes
GEO	Severe	No	Yes	Yes
Interplanetary	During phasing; other planets	During phasing; other planets	Yes	Yes

*After J. L. Barth and K. A. LaBel, NASA/GSFC

4 Space Environment Impacts

4.1 Energy Deposition in Materials

Energy deposition in materials causes radiation effects of all kinds – TID, DDD, and SEE. The ways in which different types of radiation interact with a given material and the subsequent effects manifest in electronic devices vary widely. Altering the amount of radiation exposure, the energy of a given particle, or the chosen radiation source can have dramatic effects on the results. The ways in which these changes happen are related to radiation interactions with materials. One outcome of these interactions is energy deposition. Energy is deposited by the passage of charged particles and photons through materials, either through direct or indirect processes. In semiconductor materials, that energy is converted into electron-hole pairs and/or atomic dislocations. For this short course, we will focus on the electron-hole pairs since they are the source of both TID and SEE effects. Electrons, protons, and heavy ions ($Z > 1$) deposit energy in materials through both direct and indirect ionization of the target material – *e.g.*, silicon, silicon dioxide, *etc*. In direct ionization processes, the primary (incident) particle undergoes inelastic interactions with the field of electrons surrounding the target nuclei. Small amounts of energy are given up in each collision, but there are many collisions in a typical material. Indirect ionization occurs through nuclear elastic or inelastic interactions and then the fragments from those interactions undergo direct ionization processes with the atomic electrons. There are many excellent references that cover these topics in depth. The 2006 NSREC short course by G. Santin, *et al.* [74] and the 2008 NSREC short course by R. Reed [75] have a summary of radiation interactions with materials as well as references for additional reading.

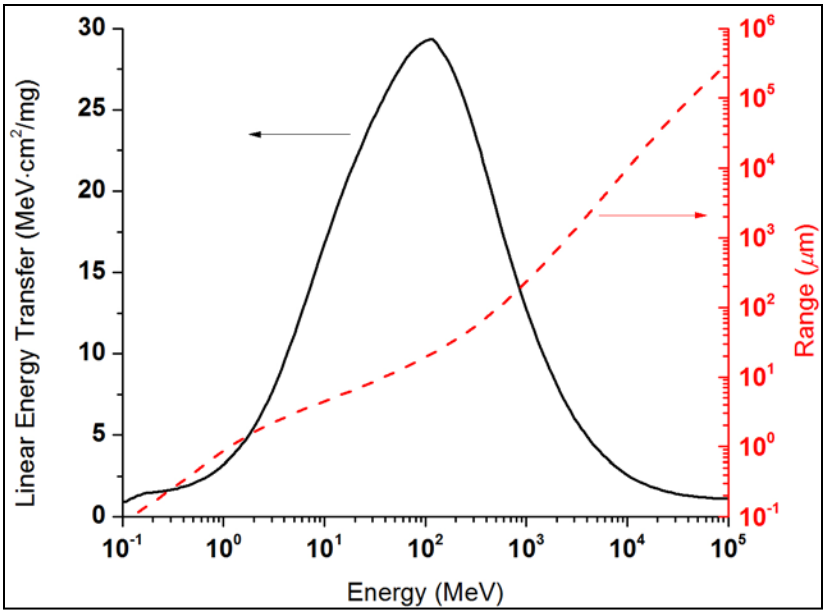

Figure 17: Direct ionization of ^{56}Fe ions in a silicon target showing the linear energy transfer (LET) and range as a function of ion energy. This output was produced using SRIM-2008 [76].

When considering direct ionization in materials, there are several derived quantities that parameterize the amount of energy that the incident particle gives up per unit length in the material. One of those quantities is called linear energy transfer (LET), which describes the amount of energy lost per unit path length of a particle as it travels through a material. LET has units of (Energy-Length^2/Mass), usually given[5] as (MeV-cm^2/mg). The base quantity from which LET is derived is called electronic stopping power[6], denoted as S and equal to $-dE/dx$, indicating energy loss per unit length – *e.g.*, MeV/cm. LET is derived by normalizing S to the material density in units of mg/cm^3 and can be quoted approximately independent of the target[7]. The LET of iron in silicon as a function of energy is shown in Figure 17. The largest LET, which occurs near end-of-range, is called the Bragg peak. The same plot could be produced for electrons, protons, and any other heavy ion in silicon or another material.

---

[5] Note that sometimes instead of "mg" in the denominator "g" is used.
[6] We have glossed over some of the details and differences between electronic and nuclear stopping power. For the purposes of this course, we shall always mean electronic stopping power and, as such, LET_{elec}.
[7] There is another quantity, related to the RPP model, called effective LET [77] E. L. Petersen, *Single Event Effects in Aerospace*. Hoboken, NJ: IEEE Press, 2011. It is the same LET discussed above, but scaled by $1/\cos(\theta)$, where θ is the incident angle of the ion. As the angle is increased towards 90°, the effective LET increases because the path length through an assumed sensitive volume shape gets longer.

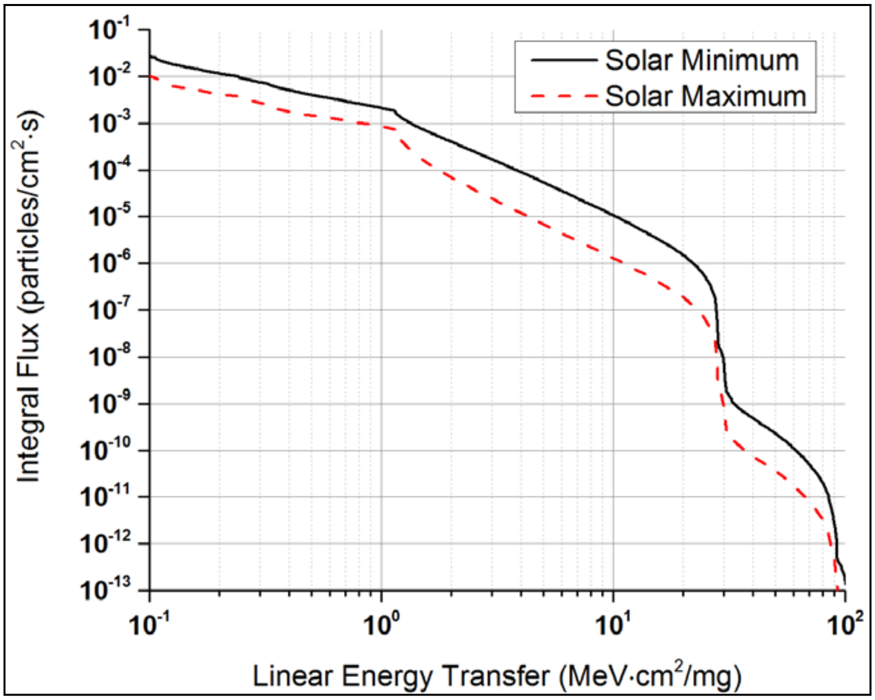

Figure 18: 1 AU omnidirectional GCR integral LET flux behind 2.5 mm of aluminum shielding, produced using the CREME96 models available at https://creme.isde.vanderbilt.edu/.

Since we know how to define LET for any ionizing particle, given its energy and the target material, we can apply this to a problem facing radiation effects engineers. Recall Figure 7 and remember that practically every naturally-occurring element in the periodic table (92 of them) is present in the space environment with energies and fluxes that vary over many orders of magnitude. A common solution to this issue combines the entire space environment into an integrated data set of ion flux versus LET, called a "Heinrich spectrum" [78]. One creates an integrated LET distribution by summing the flux for all ions for each specific LET in the target material – *e.g.*, Si, GaAs, *etc*. This technique has been discussed in detail by others; *cf.* E. L. Petersen [77].

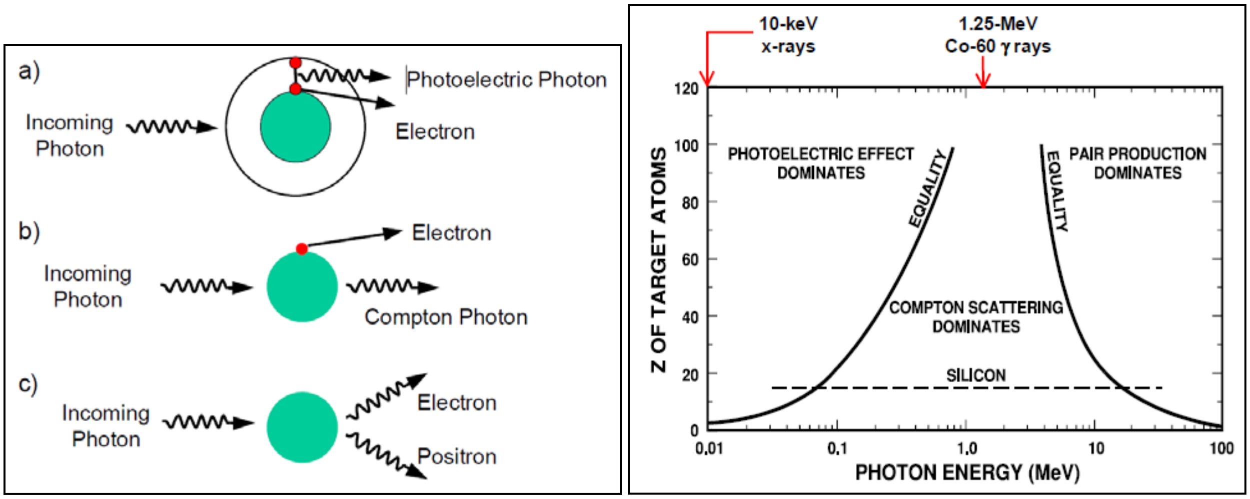

(a) (b)

Figure 19: (a) Artist's depiction of the three photon effects and their interactions with material a) photoelectric effect, b) Compton scattering, and c) pair production [79]; after J. R. Schwank, *et al*. (b) Illustration of relative importance of three photon interactions as a function of atomic number and photon energy; the solid lines correspond to equal cross sections for neighboring effects [80]; after J. R. Schwank, *et al*. Two common ground-based photon test energies, 10 keV and 1.25 MeV, are indicated.

As will become apparent in subsequent sections, photon energy deposition is an important topic for evaluating radiation effects in advanced technologies. Both x-rays and gamma rays are used for this purpose depending on the application and access to the necessary sources. When these particles are incident on a material, they generate electron-hole pairs through ionization, which are the source of almost all the induced radiation effects; the photons themselves cause little damage. There are three photon interaction mechanisms – the photoelectric effect, Compton scattering, and pair production – all illustrated in Figure 19(a). In all three cases, the end result is the production of energetic secondary electrons that in turn create electron-hole pairs. In the photoelectric effect, electrons are emitted from atoms as a consequence of their absorption of energy from electromagnetic radiation of very short wavelengths, such as x-rays. These emitted electrons are called photoelectrons. In this process, the photon is completely absorbed and excites an inner shell atomic electron to a high enough energy state that it is emitted from the atom. At that point, an outer shell electron falls in to take the place of the photoelectron, which creates a low-energy photon. Compton scattering is a type of scattering that x-rays and gamma rays undergo in matter. The inelastic scattering of photons in matter results in a decrease in energy of an x-ray or gamma ray photon, called the Compton Effect. Part of the energy of the photon is transferred to a scattering electron, which recoils and is ejected from its atom, which becomes ionized; the rest of the energy is taken by the scattered, “degraded” photon. Pair production is a process that results in the creation of an electron and a positron. A positron has the same properties as the electron, though the charge polarity is reversed. In nuclear physics, this occurs when a high-energy photon interacts with a nucleus. The energy of this photon can be converted into mass through Einstein's equation $E = mc^2$, where E is energy, m is mass, and c is the speed of light. The photon must have enough energy to create the rest mass of an electron plus a positron. The rest mass of an electron is 0.511 MeV/c^2 according to the above equation, the same as a positron. Without a nucleus to absorb momentum, a photon decaying into electron-positron pair can never conserve energy and momentum simultaneously.

In a laboratory setting, the importance of each of these mechanisms is indicated in Figure 19(b). This shows the nuclear charge of the target atoms and the photon energy ranges where each process dominates. The dashed line shows where silicon falls with a $Z = 14$ and that photons emitted from a low-energy (*e.g.*, 10 keV) x-ray irradiator will usually produce electrons via the photoelectric effect, while higher energy photons, such as gamma rays from a ^{60}Co source (1.25 MeV), will produce electrons via the Compton Effect.

4.2 Total Ionizing Dose

Total ionizing dose (TID) is the absorbed dose[8] in a given material resulting from the energy deposition of ionizing radiation. TID is a measure of the energy deposited in a medium by ionizing radiation per unit mass. It is equal to the energy deposited per unit mass of medium, which may be measured as joules per kilogram and represented by the equivalent SI unit, gray (1 Gy = 1 J/kg), or the CGS unit, rad (1 rad = 100 erg/g)[9]. The absorbed dose depends not only on the incident radiation but also on the absorbing material, so absorbed dose has to be reported as a function of target material – *e.g.*, rad(SiO_2). In advanced electronics, TID in insulating materials results in cumulative parametric degradation that can lead to functional failure. These parametric shifts can include threshold voltage shifts, increased off-state leakage, parasitic leakage paths, mobility degradation, and changes in recombination behavior affecting both MOS

---

[8] Absorbed dose should not be confused with dose equivalent or effective dose, which is reported in sieverts or rems.
[9] The radiation effects community tends to use the CGS unit, rad. 1 Gy = 100 rad.

and bipolar devices. In the space environment, TID is primarily the result of exposure to protons and electrons over a period of time, from both trapped radiation and solar particle events.

Table 4: Electron-Hole Pair Generation Energies and Pair Densities Generated by 1 rad

Material	E_p (eV)	Density (g/cm^3)	Pair Density Generated Per rad, g_0 ($pairs/cm^3$)
GaAs	4.8 (approx)	5.32	7×10^{13} (approx)
Silicon	3.6	2.328	4×10^{13}
Silicon Dioxide	17	2.2	8.1×10^{12}

*After [80]

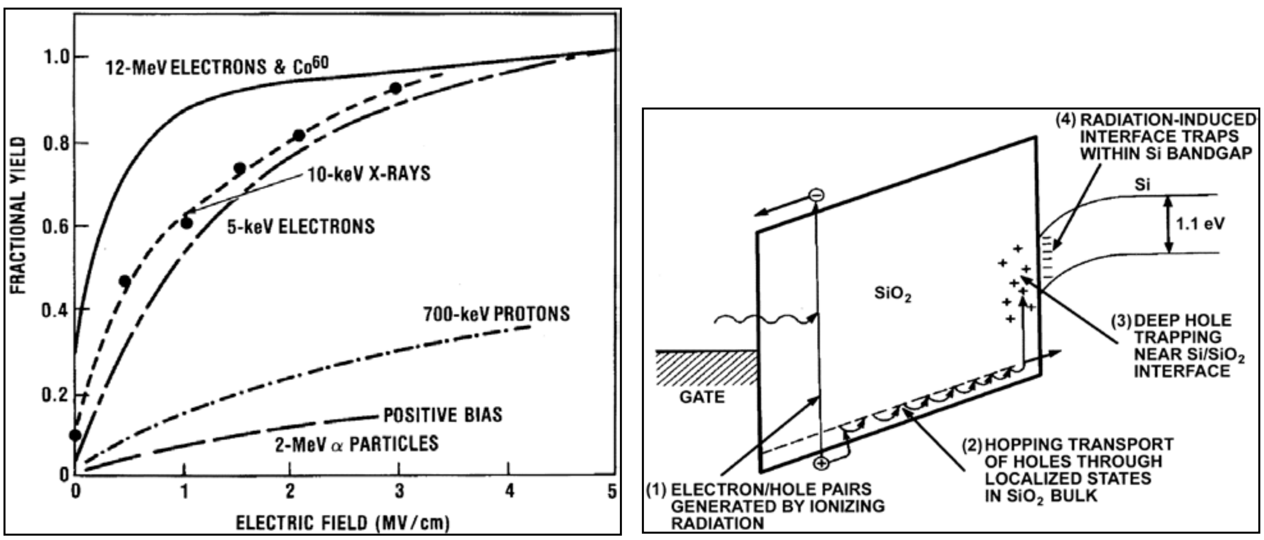

(a) (b)

Figure 20: (a) Experimentally-measured hole yield versus electric field in SiO_2 for a variety of incident particles [80]; (b) Schematic energy band diagram for MOS structure, indicating major physical processes underlying radiation response [80, 81].

The amount of damage due to ionization from electrons, ions, or photons is directly proportional to the charge yield per unit dose, which is the number of electron-hole pairs generated per rad. Table 4 lists several important electronic materials for advanced technologies and gives their average ionization energy (E_p) required to generate a single electron-hole pair as well as the initial charge pair density per rad (g_0) deposited in the target material [80]. g_0 is derived by multiplying the material density by the deposited energy per rad (1 rad = 100 erg/g = 6.24×10^{13} eV/g) then dividing by E_p. The actual charge yield in a given material is a function of the electric field and the density of electron-hole pairs created along the path of the incident particle. Figure 20(a) is a compilation of a number of experimental results of the fractional hole yield versus electric field for a number of particles spanning a wide range of LETs in SiO_2. At an electric field of 1 MV/cm, the yield varies from nearly 90% to less than 10%, indicating that charge recombination is a critical parameter for TID.

Following the creation of electron-hole pairs by incident radiation and any subsequent recombination, the leftover holes become trapped in oxide regions because their mobility is much lower than their electron counterparts [82]. These excess carriers can only accumulate and cause damage when they are trapped inside insulating layers like gate oxides and trench isolation. Figure 20(b) illustrates a MOS system and the four key underlying processes responsible for TID response [80, 81]. In the first process, the holes that escape initial recombination are relatively immobile and remain near their point of generation. In the second process, holes are transported to the Si/SiO_2 interface. This process takes place over many decades in time, and it is very sensitive to the applied field, temperature, oxide thickness, and (to a lesser extent) oxide processing history. This process is normally over in much less than 1 s at room temperature, but it can happen over many orders of magnitude if the system is at low temperature. In the third process, when holes reach the Si interface, some fraction of them fall into relatively deep, long-lived trap states, which undergo gradual annealing. The fourth major component of MOS radiation response is the radiation-induced buildup of interface traps right at the Si/SiO_2 interface. These traps are localized states with energy levels in the Si band-gap. Their occupancy is determined by the Fermi level (or by the applied voltage). Interface traps are highly dependent on oxide processing and other variables like applied field and temperature.

TID is one of the oldest radiation effects and has been studied almost since the radiation effects community was founded in the late 1950s and early 1960s [83]. During the first decade of study, from 1965-1975, we focused on understanding ionization-induced surface effects in discrete transistors. In the second decade, from 1975-1982, we concentrated on characterizing the total dose response of linear and digital microcircuits. During the third decade, from 1982-1992, we discovered that not all circuits were robust to mega-rad levels and more attention focused on advanced logic devices. Finally, from 1992-present, we have been grappling with dose rate sensitivities and the advent of enhanced low-dose-rate sensitivity (ELDRS) in bipolar devices and integrated circuits, which started with the work published by E. W. Enlow, *et al*. [84].

4.3 Single-Event Effects

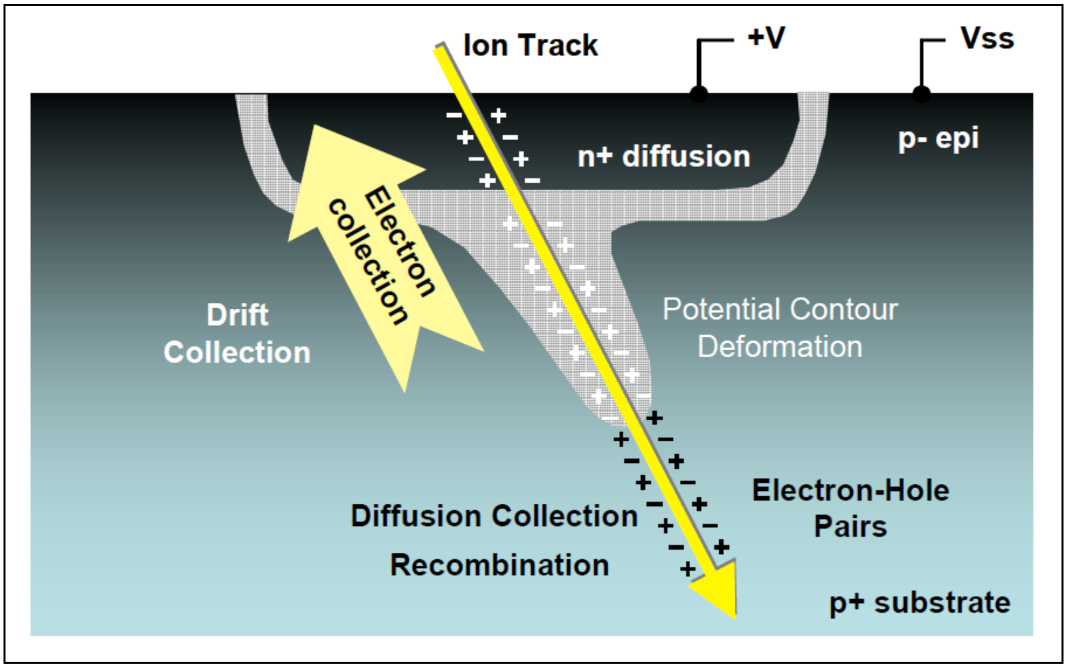

Figure 21: A schematic diagram of a reverse-biased n+/p semiconductor junction struck by an incoming ion [85]. On short time scales, electron drift collection dominates until the potential deformation collapses and the system relaxes. On longer time scales, electron collection is dominated by carrier diffusion processes from excess carriers coming from deeper in the substrate. Recombination plays a factor in each of these collection mechanisms.

A single-event effect (SEE) is a disturbance to the normal operation of a circuit caused by the passage of a single ion through or near a sensitive node in a circuit. Figure 21 shows this process in more detail, including the two charge carrier collection mechanisms: drift and diffusion. By definition all SEE are transient, though their effects within an electronic system can be lasting. SEE can be either destructive or non-destructive. Destructive SEE include single-event latchup (SEL), single-event burnout (SEB), and single-event gate rupture (SEGR). Non-destructive SEE include single-event upsets (SEU), multiple-bit upsets (MBU), single-event transients (SET), and single-event functional interrupts (SEFI). There are more event types documented in the literature, sometimes called the "SEE alphabet soup," but these are the major categories.

All SEE begin with energy deposition that results in charge generation (electron-hole pairs) in some target medium, either due to the incident particle (direct ionization) or via secondary daughter products (indirect ionization). Electrons and holes move by diffusion and drift through materials (oxides and semiconductors) to a sensitive node while they also undergo recombination. Finally, the additional charge on the circuit node alters the voltage that ultimately leads to one or more types of SEE. Depending on the environment and operational system in question, these SEE occur at some rate. The magnitude of this rate is a critical parameter for any system undergoing qualification for the space environment and is at the heart of evaluating SEE in advanced technologies.

The following is a short history of SEE, after [86]:

- The possibility of single event upsets was first postulated in 1962 by Wallmark and Marcus.
  - J.T. Wallmark, S.M. Marcus, "Minimum size and maximum packaging density of non-redundant semiconductor devices," *Proc. IRE*, vol. 50, pp. 286-298, Mar. 1962.
- The first actual satellite anomalies were reported in 1975. SEUs observed in flip-flops.
  - D. Binder, E.C. Smith, and A.B. Holman, "Satellite anomalies from galactic cosmic rays," *IEEE Trans. Nucl. Sci.*, vol. 22, no. 6, pp. 2675-2680, Dec. 1975.
- The first observation of SEUs on earth was in 1978. Observed in random access memory caused by the alpha particles released by decaying U and Th contaminants within the chip packaging material and solder. Vendors took specific actions to reduce it.
  - T. C. May and M. H. Woods, "A New Physical Mechanism for Soft Errors in Dynamic Memories," in *16th Ann. Reliability Physics Symp.*, San Diego, CA, 1978, pp. 33-40.
- The first report of SEUs due to cosmic rays on Earth occurred in 1979.
  - J. F. Ziegler and W. A. Lanford, "Effect of Cosmic-Rays on Computer Memories," *Science*, vol. 206, no. 4420, pp. 776-788, 1979.

- The first report of destructive SEE (proton-induced SEL) in a memory operating in space happened in 1992.
  - L. Adams, *et al.*, "A verified proton induced latch-up in space," *IEEE Trans. Nucl. Sci.*, vol. 39, no. 6, pp. 1804-1808, Dec. 1992.

As suggested earlier in these course notes, SEE are a more critical issue for advanced technologies relative to TID for the simple fact that for many advanced technologies the sensitive oxide volumes that can trap charge are getting unimaginably small and therefore cannot hold much charge in the first place. However, advanced technologies are generally more susceptible to non-destructive SEE than their predecessors because the amount of SEE-induced charge required to alter a latched state or cause a voltage transient to propagate is much smaller. This is the result of shrinking capacitances and what is beginning to approach countable ensembles of electrons responsible for a single device's state.

5 Evaluation of Total Ionizing Dose in Advanced Electronics

5.1 Common TID Testing Themes

In general, TID tolerance has gotten better with advanced technologies. The oxide volumes have become small enough that they cannot hold that much charge and some of the oxides are thin enough that any trapped charge is neutralized via electron tunneling. Despite those gains, device complexity has increased at a faster rate, confounding many of the attempts to perform full total dose characterizations of new components desirable for use in the space environment. This raises the question of how to test emerging technologies. As we will discuss, there are two different approaches for evaluating TID in a given device/technology: an engineering characterization and radiation hardness assurance (RHA) qualification. RHA is aimed at *qualification* given a certain set of radiation requirements – the device will either pass or fail. Engineering characterization uses the same investigative techniques and radiation sources as RHA, but there are no requirements imposed on the system and thus no pass/fail criteria. The data obtained from both methods are useful, though the latter may not be applicable to a specific program depending on that program's requirements and application-specific needs.

There are several themes surrounding TID testing in advanced technologies, including:

- ***Difficulty of in-situ evaluation;***
  - In most circumstances, it is best to "test as you fly." However, advanced technologies present many challenges on this front because application-specific testing may be very difficult if not impossible due to bandwidth limitations, some support systems in proximity cannot tolerate radiation, perhaps the device cannot be exercised or interrogated while under irradiation, and/or a sufficient number of pieces cannot be evaluated due to piece part cost or test time required.
- ***Component complexity creates "black boxes;"***
  - Many devices on the market today, like SDRAMs and microprocessors, are so complex that anyone outside of the original equipment manufacturer only has access to the high-level functions of a device. For instance, with a packaged SDRAM, it may only be possible to count errors and monitor device currents during read and write cycles, making it more difficult to correlate any observed functional failures with the available parameters. The more advanced functions and detailed information are trapped at the die level.
- ***Advanced technology material systems comprise most of the periodic table; and,***
  - We know that TID response is a function of deposited energy and the material in which the electron-hole pairs are generated. Complex material systems complicate how energy is deposited. We can still observe if a macroscopic parameter changes as a function of absorbed dose, but the mechanisms responsible for that shift may be obscured.
- ***Existing test methods for bounding predictions rely on well-behaved results and controlled starting materials.***
  - Device technology always outpaces the test methods designed to evaluate it. Test methods usually rely on controlled starting materials for the test, meaning that the person or group conducting a TID test can segregate the material into wafer/diffusion lots. Manufacturing lots, which is where the packaging lot-date-

code comes from, can contain more than one wafer lot unless the packaging process is controlled by a procurement specification. Multiple wafer lots in a single test sample can result in a large data spread. The spread in the data can be uni- or multimodal, further complicating analysis.

5.2 Available TID Test Methods

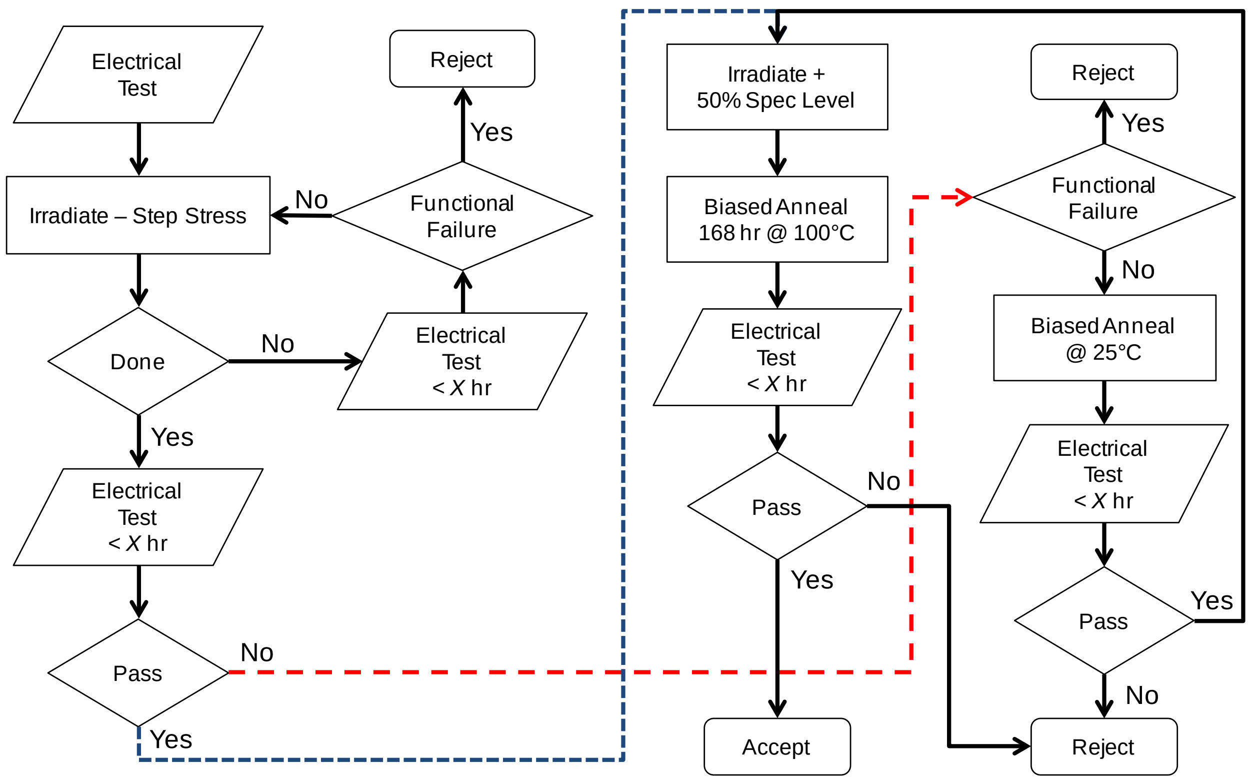

Figure 22: Test flow for MIL-STD-883, Test Method (TM) 1019. The time in which electrical testing must be performed between irradiation steps can vary within the context of TM 1019.8, so it is left as a variable in this context. Figure adapted from [87]. Removal of the pass/fail criteria is one way to descope this method into an engineering characterization.

TID testing is performed to determine the type and magnitude of a device's parametric degradation and to check for functional failures. This is done to calculate the suitability for a radiation environment. Ground-based TID testing is carried out with an ionizing radiation source that can include photons from an x-ray or gamma ray source, electrons from linear or Van de Graaff accelerators, or protons from cyclotron, synchrotron, or Van de Graaff accelerators. In most cases these ionizing radiation sources are highly-penetrating by design to maintain charge particle equilibrium throughout the target, so advanced device preparation is not necessary.

There are two general methods in use for TID testing: one from the United States based on MIL-STD-883, Test Method 1019 ("IONIZING RADIATION (TOTAL DOSE) TEST PROCEDURE") and one from Europe based on the European Space Components Coordination (ESCC) Basic Specification No. 22900 ("TOTAL DOSE STEADY-STATE IRRADIATION TEST METHOD"). Both of these methods are similar, though there are subtle differences. The method that gets utilized depends on programmatic decisions. Given a set of requirements, these methods can be used for qualification – pass/fail – purposes. In the absence of requirements, these methods provide a framework for engineering characterization. A graphical representation of MIL-STD-883, Test Method 1019 is shown in Figure 22.

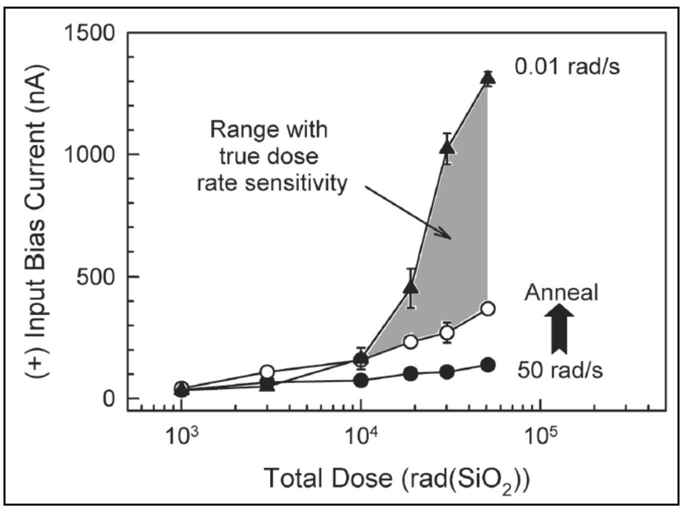

Figure 23: I_{B+} versus total dose for LM111s subjected to a 175°C, 300-hr pre-irradiation elevated temperature stress. The devices were irradiated at 0.01 (triangles) and 50 rad(SiO_2)/s (circles) with all pins shorted. Following the 50 rad(SiO_2)/s irradiation, the devices were annealed at room temperature with all pins shorted for a time equivalent to the low dose rate irradiation (open circles). ELDRS is evident by comparing the triangles and open circles. Figure and caption after [88].

For bipolar/BiCMOS devices and circuits, each of these test methods has procedures to address EDLRS. Figure 23 shows an example of ELDRS for voltage comparators irradiated at both high and low dose rates. The LM111s irradiated at low dose rates exhibit much more degradation in the input bias current than LM111s irradiated at high dose rate and then annealed at room temperature for a time equivalent to the low dose rate irradiation for the same total dose. This true dose rate effect is indicated by the shaded region in Figure 23. While ELDRS is usually limited to bipolar and BiCMOS technologies, dose rate effects are a key component to evaluating advanced technologies.

5.3 TID Test Issues for Advanced Technologies

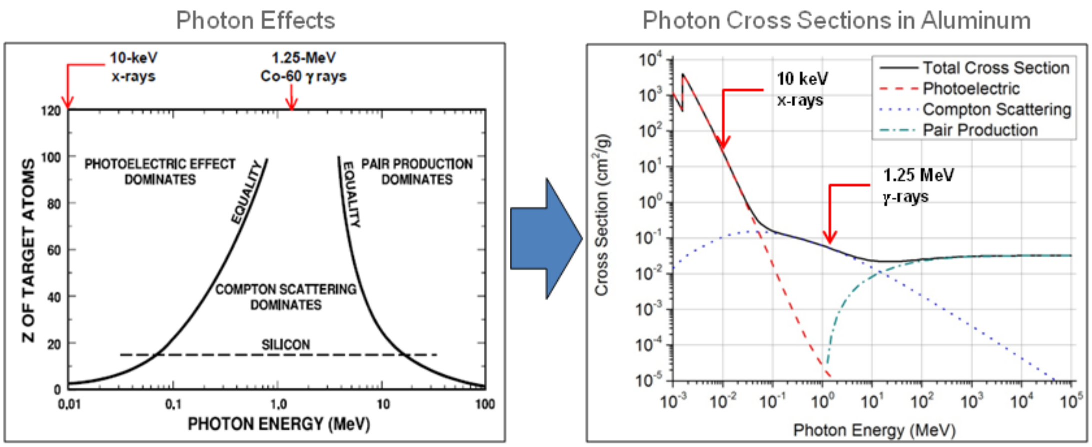

Figure 24: This figure is partially based on a chart shown in Figure 19, but it shows specific photon cross sections for aluminum, which is a common shielding material. One can see that 10 keV x-rays are much more readily absorbed via the photoelectric effect than gamma rays via the Compton Effect.

We have many radiation sources to choose from when doing ground-based TID testing, including photon, electron, and ion sources. Photon sources are very common because they are cost-effective and provide an easily calculable (and controllable) dose rate. X-ray sources, such as ARACOR irradiators, provide a source of 10 keV x-rays. Gamma ray sources, like ^{60}Co, provide a source of 1.25 MeV gamma rays. ^{60}Co is a synthetic radioactive isotope of cobalt with a half-life of 5.27 years. It is produced artificially by neutron activation of the isotope ^{59}Co. ^{60}Co undergoes beta decay to the stable isotope ^{60}Ni. The activated nickel nucleus then emits two gamma rays with energies of 1.17 and 1.33 MeV, the average energy of which is approximately 1.25 MeV. Figure 24 shows photon interaction mechanism cross sections versus energy for aluminum, which is a common shielding material and often found in the back-end-of-line (BEOL) of semiconductor processes. For example, in aluminum, the photon intensity drops to 50% after 1 mm for 10 keV x-rays and after 5 cm for 1.25 MeV gamma rays – a 50x difference. This means that, while gamma rays are harder to shield, they offer more uniform penetration and charge generation through packaging and semiconductor materials. Consequently, x-rays are often limited to irradiation at the die level, though even that can present a challenge if the technology has a full BEOL build of 9-12 levels of metal.

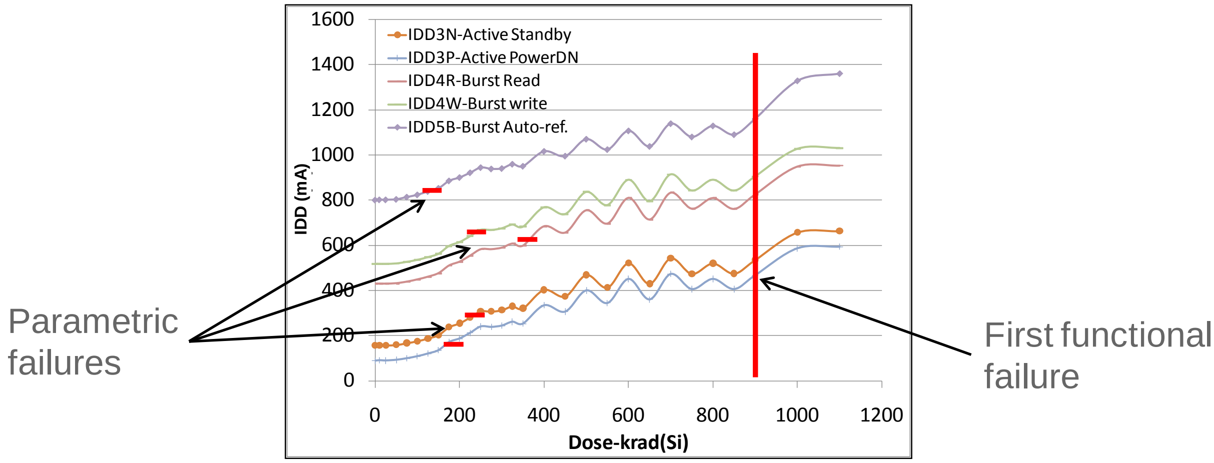

Figure 25: Samsung DDR2 SDRAM under TID irradiation with ^{60}Co gamma rays to 1.1 Mrad(Si). The initial parametric failures and the first functional failure are shown [89].

"Black-box" components present another issue for testing advanced technologies. The DDR2 SDRAM data shown in Figure 25 are indicative of this problem. For a SDRAM like this, supply currents are one of the few metrics that can be tracked during irradiation. The parametric failures occur at 150 and almost 400 krad(Si) for the different supply lines. However, the first functional failure didn't happen until 900 krad(Si). The question is whether or not supply current is a good predictor of functional failure and will the margin between parametric and functional failure be maintained for this process across manufacturing lot date codes? The same issues could present themselves for other advanced devices like NAND flash, FPGAs, and microprocessors.

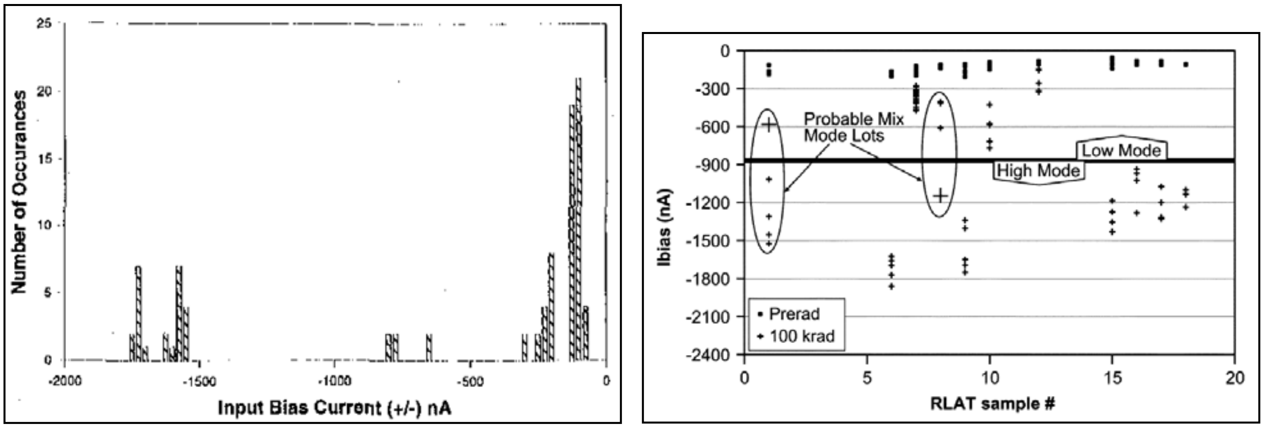

(a) (b)

Figure 26: (a) histogram of input bias currents at 50 krad(Si) for low dose rate irradiations of the LM111 voltage comparator [90]; (b) OP484 I_{bias} versus lot sample after 100 krad(Si) at low dose rate. [91].

Component variability, in addition to radiation source and parametric monitoring constraints, presents another TID testing challenge for advanced technologies. Two issues exist: 1) many of these advanced devices are commercial and the wafer materials are not controlled within a manufacturing lot, and 2) even if the wafer material is controlled, the process can introduce variability into the test results. The latter is manifest in the two data sets of Figure 26. These data are bimodal, though some data sets can have more than two modes. Sampling strategies for radiation testing often represent a compromise between generality and economy [31, 91]. The most general strategies assume little about parts' radiation response distributions. However, such strategies require large samples to achieve high confidence of high success probability for many types of distributions, well-behaved and multimodal alike [91]. More economical strategies begin with the assumption that the radiation response within a wafer lot should be consistent from part-to-part, like those in MIL-HDBK-814, and assume the radiation response distribution will approximate a particular form. This allows the establishment of higher success probability and confidence with smaller test samples. In many cases, like those shown in Figure 26, these small sample size assumptions are violated and the ill-defined tails in the distribution(s) dominate the risk. Because small sample sizes do little to constrain the tails of the data distribution, it is nearly impossible to identify pathological behavior. For advanced technologies, economics often drive sample size, but every effort must be made to combat this, particularly for qualification testing.

There are many other issues that could be included in this discussion. For instance, we have not spent much time discussing actual characterization techniques. For many advanced technologies, self-heating is a major issue when the device is under bias. This is particularly true for discrete FETs under test in deep submicron technology nodes. Pulsed *IV* techniques are needed to avoid systematic errors in data collection that can cloud the actual radiation response. Current testing challenges will continue and new obstacles will arise as the market continues to diversify and grow.

5.4 Possible TID Testing Solutions

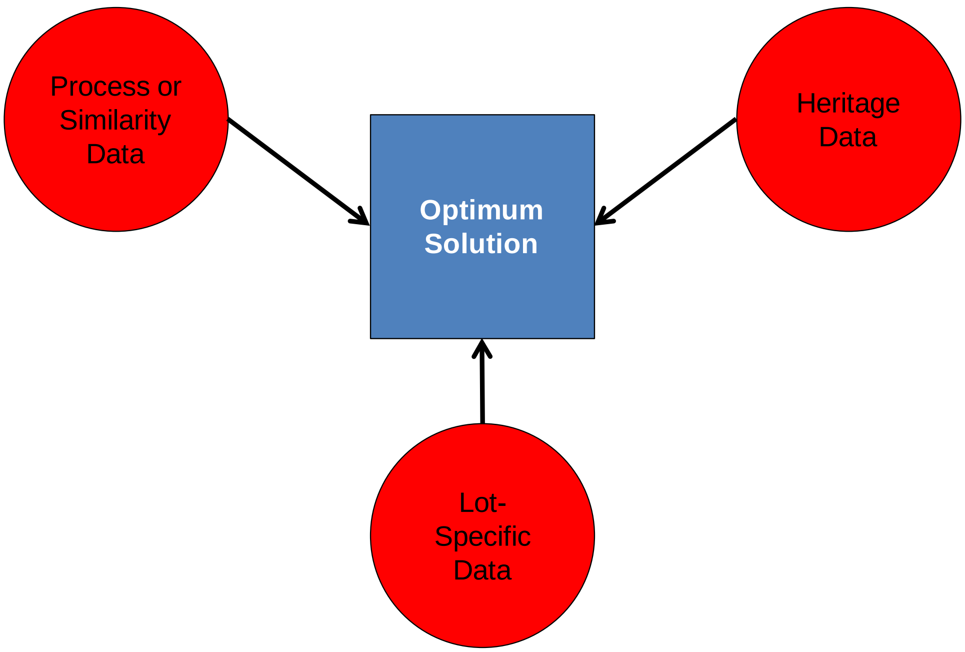

Figure 27: A Bayesian approach for total ionizing dose hardness assurance, facilitating the incorporation of disparate data sources, as described by R. L. Ladbury, *et al*. [92]. In this case, "lot-specific" data refers to wafer-lot-specific data, not the packaging/manufacturing lot date code.

In an ideal world, we would have the necessary and sufficient wafer lot data for all the technologies we intended to deploy in the space environment. However, engineers and scientists in this field will tell you that's rarely the case. More often than not, we are forced to make decisions with less than perfect information. R. L. Ladbury, *et al*. suggested a new methodology using a Bayesian approach for probabilistic risk assessment for improved qualification and risk assessment [91-93]. It is described graphically in Figure 27 and facilitates the incorporation of all available data types. This set of techniques shows improvement as data are added, which can be done at any stage of the qualification process. The Bayesian methodology defines a methodical way to incorporate generic data from other groups and may in fact encourage data sharing. This type of flexibility and leverage will be critical as more low-cost, high-performance platforms, like cubesats and smallsats, are put into plan and fielded.

Other possible TID test solutions for advanced technologies include:

- Exploring the feasibility of non-photon radiation sources in some cases;
- Developing flexible interrogation methods for advanced, large-scale integration devices;
- Increasing lot test size to the maximum practical extent;
- Testing components to failure whenever practical;
- Leveraging as much existing data as possible; and,
- Tracking basic mechanisms research to maintain knowledge base on advanced material systems and the latest simulation techniques.

These techniques are aimed at constraining the degradation and failure distributions of the components under test so that statistical analysis can still take place.

6 Evaluation of Single-Event Effects in Advanced Electronics

6.1 Common SEE Testing Themes

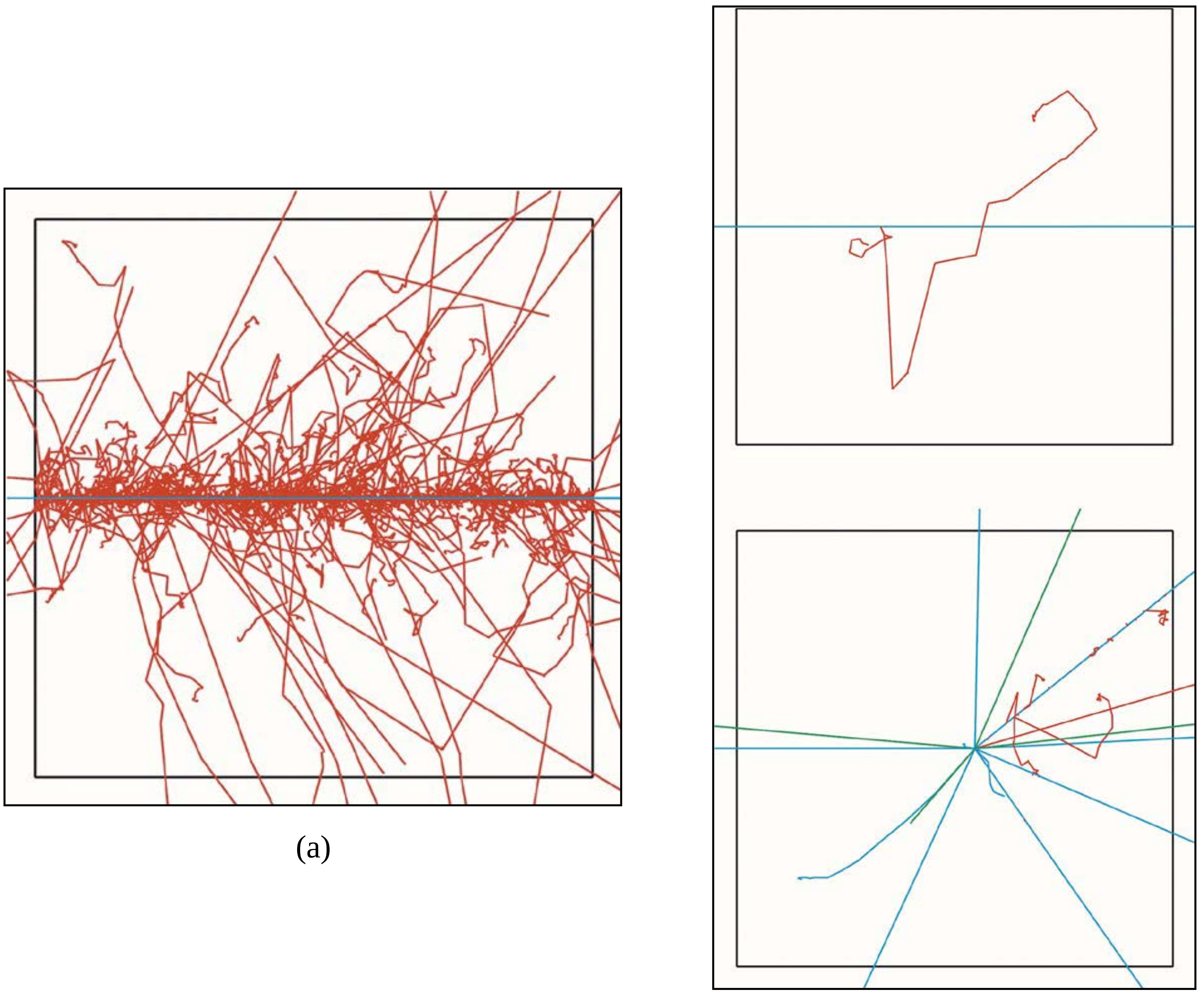

(a) (b)

Figure 28: (a) 100 MeV protons in a 1 μm silicon cube; (b) 1 GeV protons in a 1 μm silicon cube. Figures after [94]. These events were generated using the Geant4-based MRED tool [95].

A common theme for SEE in advanced technologies could be, "*the death of averages*." So many of the traditional techniques and standards used to evaluate SEE in a given component or technology relied on statistical averages over many individual events, like LET. The proton event images in Figure 28 are a simple demonstration of how non-average a typical single event can be. When technology feature sizes were large compared to the size of a radiation event, averages like the continuous slowing down approximation range and LET worked because the size of the transistors "integrated" the radiation effects. However, as we have progressed to transistors fabricated in 32, 22 nm, and smaller process nodes those integrating effects are no longer there and the features present from one event to another contribute substantial differences. SEE caused by high-energy electrons, called delta rays, are a great example of this – *cf*. [96].

Beyond this initial discussion, many of the same issues present for TID testing of advanced technologies are also present for SEE testing. This includes complications due to in-situ evaluation and "black box" components. However, since SEE also depend on additional factors of the incident radiation, the parameter space gets larger. For instance, in the past several years, there have been a number of investigations that highlighted the angular sensitivity of deep submicron technologies – *cf*. [97-100]. Beyond that there have been a number of papers discussing SEE sensitivity in scaled CMOS to direct ionization by low-energy protons [19-23, 101-103]. This had been postulated for a number of years, but was not experimentally observed and reported on until 2007 [101]. Beyond the low-energy protons, there has been recent work that indicates muons can cause SEE, which will become an issue for terrestrial electronics since there is a substantial muon flux at ground level due to atmospheric cosmic ray showers [104, 105]. In general, the parameter space is enormous and not getting any smaller, which begs the question of how to test advanced technologies while ensuring that risk is bounded.

6.2 Available SEE Test Methods

We perform SEE testing to determine the *presence and characteristics of* single events, which can include destructive or non-destructive effects, voltage and temperature dependence, as well as measurements of the amplitude and width of SETs. We also perform SEE tests to *calculate the SEE rate* for a radiation environment. SEE testing is normally conducted at particle accelerator facilities that use cyclotrons or tandem Van de Graaff machines, which irradiate the whole device with ions (protons or heavy ions). Some of these facilities offer operation in-air, while others require irradiations to be performed in-vacuum due to energy/range limitations of heavy ions. Furthermore, since most heavy ions only have ranges up to several hundred micrometers in silicon, packages must be opened and the devices de-processed and/or thinned to ensure adequate penetration into and through the active regions. In some cases, correlated spatiotemporal information is needed, which requires a focused ion beam (*e.g.*, microbeam) or a pulsed laser source.

Again, like TID, there are several SEE testing methods available to the community. However, even in the most specific cases, these documents can only be considered guidelines, perhaps with the exception of MIL-STD-750, Test Method 1080. Single-event testing is too application-specific and the parameter space too large for a single method to encompass all techniques in a self-consistent way.

- ASTM F1192: Standard Guide for the Measurement of Single Event Phenomena (SEP) Induced by Heavy Ion Irradiation of Semiconductor Devices
    - Last updated/affirmed: 08/2006
- ESCC Basic Specification No. 25100: Single Event Effects Test Method and Guidelines
    - Last updated/affirmed: 10/2002
- JESD57: Test Procedure for the Management of Single-Event Effects in Semiconductor Devices from Heavy Ion Irradiation
    - Last updated/affirmed: 12/1996
- JESD89: Test Method for Beam Accelerated Soft Error Rate (terrestrial effects)
    - Last updated/affirmed: 01/2012
- MIL-STD-750, Test Method 1080: Single-Event Burnout and Single-Event Gate Rupture
    - Last updated/affirmed: 01/2012

All of these methods do a reasonable job for general purpose heavy ion testing, but they do not cover proton SEE (low-energy or otherwise) nor recently-reported phenomena such as extreme angular sensitivity and situations in which heavy ion indirect ionization dominates SEE rates.

We outline the steps to perform a SEE test using the guidelines below:

- Understand the device process technology and application conditions – SEE testing is most always application-specific;
    - It is important to understand if the device under test is susceptible to destructive SEE, like latchup in a bulk CMOS technology. This will dictate how testing is set up and proceeds.

    - Is there a target environment for qualification (requirements) or is the test an engineering characterization? The answer to this question may dictate parameters like maximum LET and heavy ion/proton fluence.
- Identify a suitable test facility and consider systematic variables;
    - Systematic variable include ion selection, pulsed laser sources, energy range, flux range, dosimetry, beam profile and purity, and accelerator technology for beam structure consideration if the testing is dynamic.
    - Though it is beyond the scope of this work, pay particular attention to facility-provided dosimetry. There are numerous anecdotes where a team found out that calibration factors were off (unintentionally, of course) by a decimal place and caused them to irradiate their parts 10x beyond the mission requirement. *Caveat emptor!*
- Develop a test matrix that covers the necessary application space within allowable costs;
    - This application space can include device function, data patterns, frequency, voltage/current, temperature, LET, energy, range, *etc.* Many of these parameters can have large ranges.
- The majority of time before, during, and after a SEE test is spent on just a few items; and,
    - Deciding what you want to measure and how;
    - Verifying you can do the former; and finally,
    - Figuring out what you actually got.
- Because SEE testing is real-time, many aspects are dynamic, so contingency planning is essential.
    - Always have a backup plan to avoid wasting time, labor, and beam costs.

6.3 SEE Test Issues for Advanced Technologies

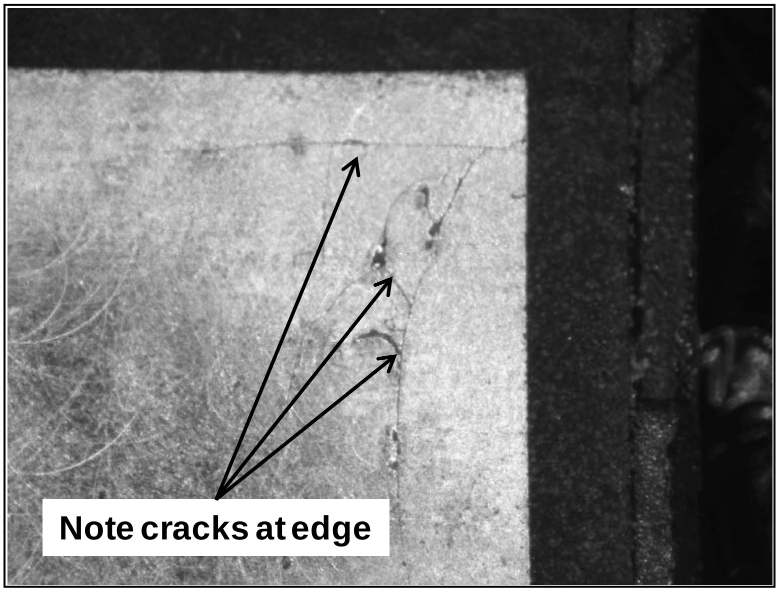

Figure 29: Thinning of a Samsung DDR2 SDRAM resulted in cracking of the die. Special precautions were needed to achieve acceptable yield for part thinning (Courtesy of Aeroflex/RAD) [106].

One of the key issues that differentiates SEE testing from TID testing is device preparation. Heavy ions cannot penetrate through the same amount of material that is typically encountered with ^{60}Co gamma rays or high-energy (~200 MeV) protons. For top-side wire-bonded components, we compensate for short ion range by mechanically or chemically removing package lids and plastic encapsulant. For C4/flip-chips that have land grid or ball grid arrays, the device's substrate must be thinned in addition to de-processing of the package. An example of this is shown in Figure 29, where a DDR2 SDRAM was destroyed during de-processing and substrate thinning procedures. Maintaining yield with a human-based mechanical process is not trivial and can impact the number parts available for testing, which can drive up statistical uncertainty if destructive effects are suspected.

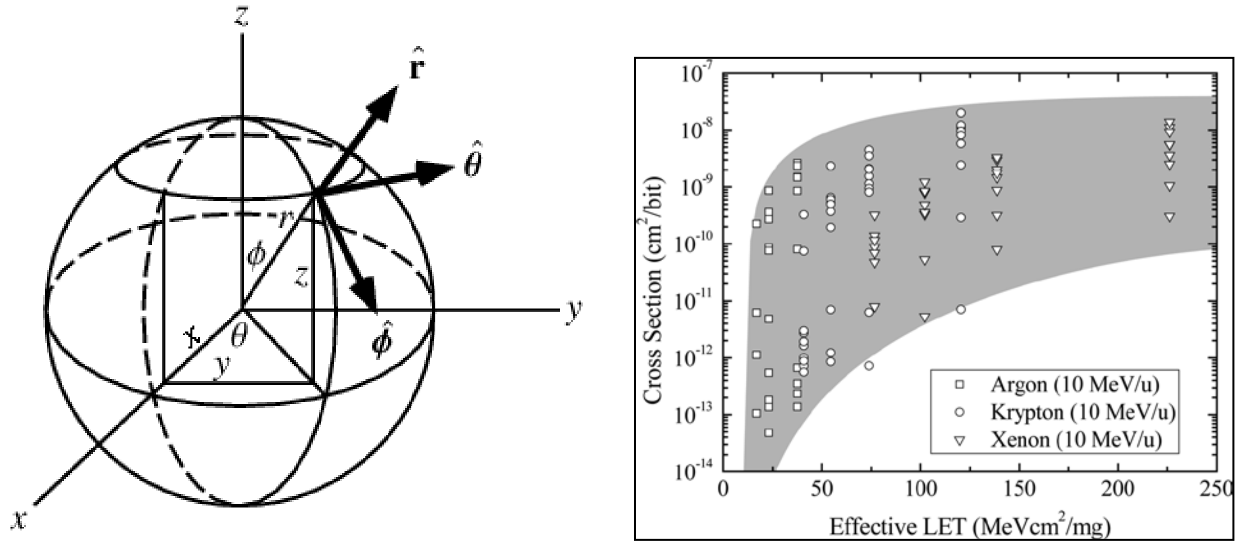

(a) (b)

Figure 30: Spherical coordinate system after http://mathworld.wolfram.com/SphericalCoordinates.html/; (b) compilation of heavy ion data from irradiation of a latch shown in the classical effective LET manner. The span of SEU cross section for a given LET is due to the dependence of cross section on roll angle [97].

Traditional SEE test methods incorporated angled irradiations to increase the effective LET, assuming the sensitive volume does not have a high aspect ratio and obeys 1/cos(θ) scaling – *i.e.*, it works well for a pancake and not so well for a pencil [77]. However, as advanced technologies have gotten more sensitive and the transistors packed closer together, single ions can affect larger portions of system. This means that simple tilt irradiations are insufficient. The diagram and data set in Figure 30 demonstrate why investigating both tilt and roll angle[10] are vital for proper understanding of the device under test. In that data set alone, at some of the lower effective LET values, the cross section varies by almost 5 orders of magnitude as a function of roll angle. The combination of tilt and roll angle have also been identified as important parameters for SEL [100, 107] and MBU [98] SEE tests of advanced technologies.

[10] Assume the beam velocity is moving in the -*z* direction. Tilt angle is defined as deflection of the polar angle (φ) relative to the beam velocity. Roll angle is defined as deflection of the azimuthal angle (θ), which is perpendicular to the beam velocity.

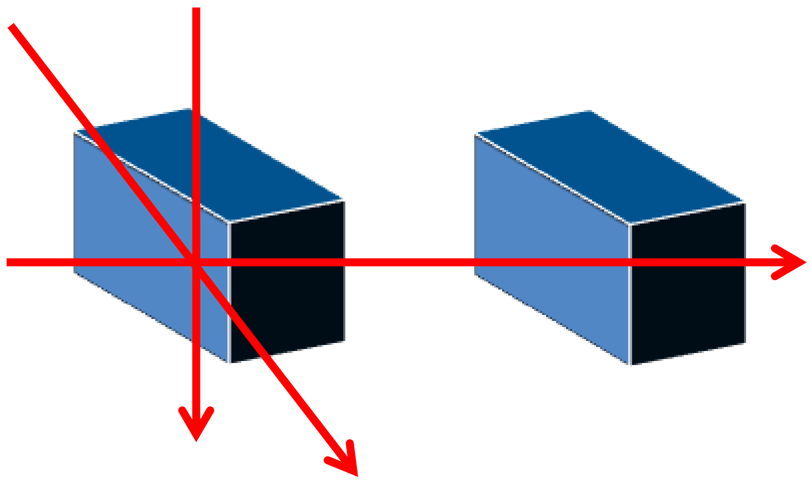

Figure 31: Two notional sensitive volumes in a device under test. The beam vectors show possible irradiation conditions that can affect one or both of the volumes.

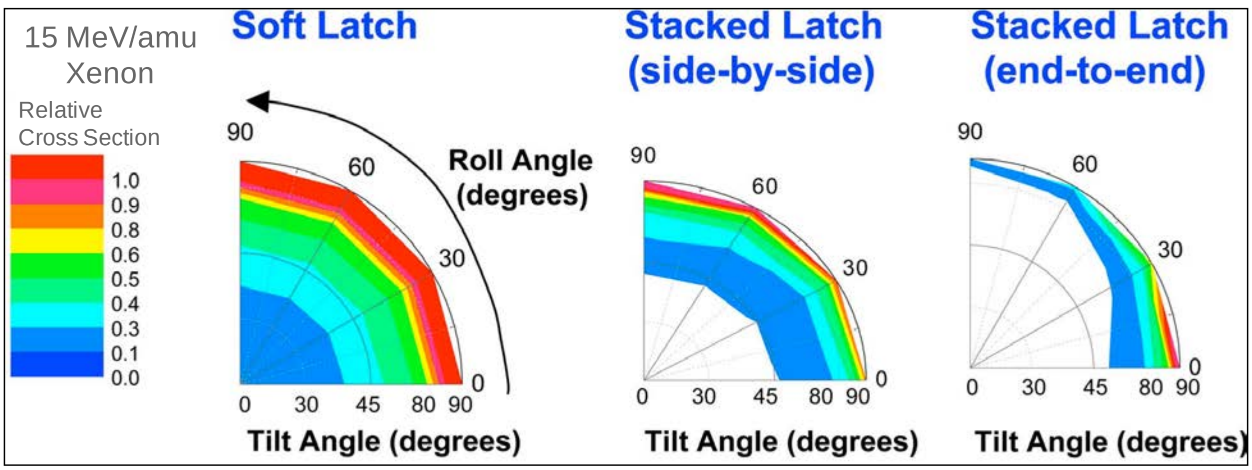

Figure 32: Normalized angular dependent cross section distributions for Xe 15 MeV/amu for a 32 nm SOI latch. The Xe plots were normalized to the highest Xe cross section [19]. These plots are the result of data-informed simulations.

Over 50% of the space environment is incident at angles greater than 60°, so understanding the angular sensitivity of a candidate device is important [40]. Figure 31 and Figure 32 represent some interesting findings from various designs of a two-stage latch fabricated in a 32 nm SOI process and irradiated with 15 MeV/amu xenon ions. The soft latch behaves rather symmetrically as its angular dependent cross section distribution is sampled through the first octant of a sphere. However, latch designs that incorporate different types of RHBD techniques do not respond symmetrically, which impacts the overall device cross section and has implications for SEE rate calculations. The manner in which ions cross through the sensitive volume(s) dictates how a circuit responds. Figure 31 shows some variations on this, all of which may produce different effects at the circuit-level. Making sure to sample that response is critical and will continue to be one of the more difficult aspects of SEE testing.

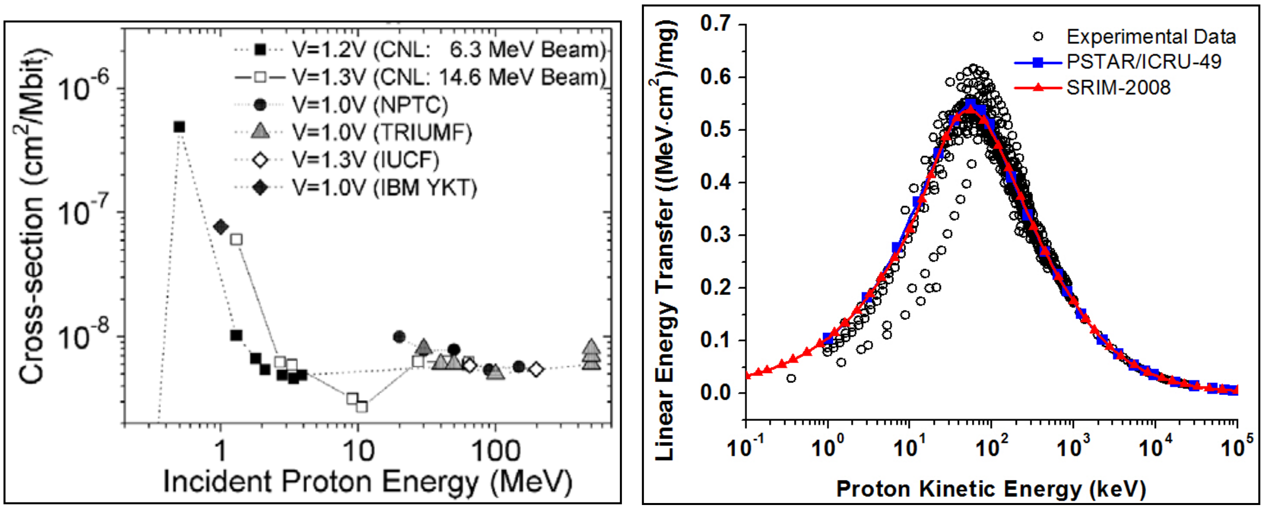

(a) (b)

Figure 33: (a) proton-induced SEU data from 1 MeV to 500 MeV on a 65 nm SOI SRAM [102]; (b) LET data [108] and simulation results for protons in a silicon target.

Low-energy, proton-induced non-destructive SEE are one of the more significant issues to emerge in the past five years within the radiation effects community. It appears that as technologies continue to scale, the low-energy proton sensitivity is only going to increase. The upset mechanism is direct ionization from the primary particle at low energies, when its LET is large enough to deposit sufficient energy in a sensitive volume that a latched state is altered or a transient is generated. This effect is shown in Figure 33(a) when the primary proton energy drops below roughly 2 MeV and cross section increases by more than 10x. There are other examples of this in the literature [19, 20, 22, 23, 101, 109, 110].

Unfortunately, testing with low-energy protons is not as straightforward as would be the case with high-energy heavy ions with similar LETs and much longer ranges. A proton close to stopping, when its LET peaks, only has an average range of 0.5 μm, making it very hard to place that Bragg peak inside the sensitive volume of device under test after its energy has been degraded by the beam line materials and the device under test itself. Increased LET variability at the Bragg peak introduces additional statistical and systematic variability. The increase in LET variability is due to energy straggle, which is unavoidable unless the amount of material that the beam passes through is minimized between the acceleration source and the sensitive volume. These problems are compounded with flip-chip devices, which are used extensively in advanced technologies that require high levels of on-chip integration and user input/output. That being said, Monte Carlo simulation toolkits can provide a path forward provided that the simulation environment is accurate and the proper physics are included.

For hardness assurance and evaluation purposes, the following are reasonable suggestions for characterizing a device's response to low-energy protons [22]:

- Measure the upset cross section with long range, low-LET light ions;
    - This assumes that proton LET is the right metric for the cross comparison with heavy ions.
- Create an event model using low-LET data and whatever technology information can be gathered;
    - This step may require assumptions.
- Validate the model by comparing it with measured low-energy proton response; and,
    - Based on experience gained so far, we have the following recommendations:
        - Measure and record materials in the beam line upstream from the device-under-test. Higher density and atomic number increase the importance of these materials for subsequent transport calculations.
        - Experimentally determine the mean beam energy and beam energy-width at the device-under-test location. This should be carried out for the primary, un-degraded beam as well as for all degraded beams. Accurate and precise knowledge of the beam energy is critical for subsequent transport calculations since differences in beam energy on the order of 100 keV can result in single-event upset cross sections different by more than an order of magnitude.
        - In reference to the first item, it is important to complete transport calculations using accurate and properly ordered material stacks. It is

inadvisable to collapse identical materials appearing in different upstream locations. As a proton slows down, its stopping power increases non-linearly, so transporting a proton through an aluminum-air-aluminum stack is not the same as an aluminum-air stack with equivalent thicknesses.

  - Different levels of systematic error in the form of energy loss straggling can be introduced depending on the type of device-under-test package. Top-side wire bond schemes are preferable since the semiconductor back-end-of-line process is thin. Controlled collapse chip connection (C4), or flip-chip, packages are more common for commercial, highly-integrated parts. Flip-chip parts require irradiation through the backside of the die – *i.e.*, substrate – and should be uniformly thinned if possible to reduce straggling and lower the energy of possible beam tunes. Thicknesses less than 100 μm are preferable, but are fraught with their own set of challenges. All parts must be de-lidded.
  - In reference to item above, if the die is thinned, variations in proton stopping power can occur in different regions of the device if the die thickness is not uniform. The single-event upset cross section can be altered by variations of less than 10 μm of material. Mitigating this problem requires two things: knowledge of die thickness and a way to monitor the physical location of single-event upsets. Die thickness can be determined non-destructively via x-ray cross sections or Rutherford backscattering spectrometry or, alternately, through destructive physical analysis following the experiment. Knowledge of physical upset location is achieved more easily for SRAM arrays, but can be quite challenging for more complex devices such as SDRAMs and FPGAs. This topic should be incorporated into the test design.

- Use the calibrated model to predict the on-orbit error rate using an appropriate radiation transport tool set.

Figure 33(b) shows experimentally-measured proton LETs in silicon as well as different electromagnetic physics simulation packages. The simulations agree well with the majority of data presented, though the large spread in experimental LETs below 1 MeV is apparent. It is generally true that experimental errors in measured stopping powers increase with decreasing energy [111-113]. For transmission measurements at low energy, thin foils are needed. This makes the presence of pin holes, surface impurities, and thickness variations detrimental to the measurement. Furthermore, the critical angle for channeling increases at low energy along with the importance of multiple scattering. These facts translate to uncertainty in stopping power formulations that rely on these data, which includes SRIM [76, 114-116] and codes based on ICRU Report 49 [117], such as Geant4 [118, 119]. Nevertheless, simulations guided by careful experiments are the most likely solution to study low-energy proton SEE.

Beyond low-energy protons, there are a whole host of other particles that can contribute to SEE in advanced technologies as they become more sensitive to radiation-induced energy deposition. Recent investigations have added muons and delta rays to the list of possible radiation sources capable of inducing SEE [96, 104, 105]. With the ever increasing particle count, mechanism list, and the size of the experimental matrix, the importance of informed device, circuit, and system-level simulations will increase. In many cases, Monte Carlo radiation transport simulations may be the only way to manage the tens or hundreds of dimensions that must be sampled to analyze radiation effects in advanced technologies.

6.4 SEE Rate Calculations

Table 5: Key Milestones in the Development of SEE Rate Prediction Methods

Milestone	Date	Authors
First reported SEU in space	1975	Binder, Smith and Holman
LET distribution concept is introduced	1977	Heinrich
First reported alpha particle upset in ground-based ICs	1979	May and Woods
Development of heavy ion SEU rate prediction model based on distributions of path length and LET	1978, 1980	Pickel and Blandford
First observations of proton-induced SEU	1979	Wyatt, McNulty, Toumbas, Rothwell and Filz Guenzer, Wolicki and Allas
Development of semi-empirical model for proton SEU rate	1983	Bendel and Petersen
CRÈME suite of codes combine environment and rate prediction tools in standardized package	1986	Adams
Development of Effective Flux approach for heavy ion SEU rate	1988	Binder

*After R. A. Reed, *et al.* [120].

Table 5 gives some key milestones in the development of SEE rate calculations techniques. Today there are many packages available via web-interfaces as well as standalone executables that run on a personal computer. Most modern analytic tools used for on-orbit rate evaluation incorporate environment calculations and the direct ionization SEE rate calculation into the same platform. These tools convolve the predicted space environment (usually a "Heinrich spectrum" for heavy ions) with a response function for the device under simulation. The procedure is similar for proton indirect ionization rate calculations, though the starting environment and response function are parameterized differently.

These analytical tools are ideally suited for many problems, but they fall short in some specific cases that can impact advanced technologies [95, 121]:

- Angular dependence with protons or heavy ions that violates $1/\cos(\theta)$ scaling;

- Low-energy proton or non-heavy ion effects (delta rays, muons, *etc*.);
- Bipolar amplification effects in SOI CMOS;
- Charge collection by diffusion;
- Heavy ion indirect ionization;
- Ion track structure effects; and,
- Thick sensitive volumes.

If one or more of these issues is present in a system or device under evaluation, traditional SEE rate calculation methods will not yield an accurate answer. More advanced Monte Carlo techniques are required to add additional physics and a better physical description of the system under simulation. Monte Carlo simulation provides a path forward since an analytical solution is not required. It can invoke [21, 95, 122-124]:

- Quantitative description of the relevant radiation environment(s);
- Transport of the incident radiation through any materials or structures that surround the sensitive circuitry;
- Energy deposition in the electronic materials by the impinging radiation;
- Conversion of energy into charge;
- Charge transport and recombination in the semiconductor and insulator regions;
- Transistor-level response, including effects of charge deposited by incident radiation; and,
- Circuit response, including radiation-induced transients.

6.5 Possible SEE Testing and Rate Calculation Solutions

There are many possible solutions to improve SEE testing and rate calculation accuracy for advanced technologies, though in general it simply requires more thought and planning. Keep the following guidelines in mind when considering SEE in advanced technologies:

- Develop advanced skills to de-process and prepare devices for testing;
    - There are different requirements for protons, heavy ions, and laser irradiation along with various mechanical and chemical methods.
- Study facility capabilities and understand the limitations of each;
    - You are your own best advocate.

    - This is particularly true when evaluating low-energy proton, delta ray, and muon-induced effects.
- Utilize test methods that yield intimate device control and data visibility;
- Develop a clear understanding of data capture and analysis requirements; and,
    - This will save time and help communication amongst team members and benefit your project when it comes time to calculate operational SEE rates in a given environment.
- Study the available SEE rate calculation methods and understand their limitations and what you're asking the tool to return.
    - The answer is only going to be as good as the question asked.
    - This may mean running both analytical and Monte Carlo simulations for comparison purposes.

7 Future Challenges

I covered a lot of ground in this short course, starting with a brief survey of advanced electronics and then moving into a description of the space radiation environment. We discussed how the space radiation environment induces different types of radiation effects like total ionizing dose and single-event effects. These topics included many common themes and echo the same types of difficulties. Advanced technologies stand to enable the next generation of space systems if we can understand how to utilize them safely. I am a firm believer that we have the tools, knowledge, and facilities to conquer the challenges laid out. Future endeavors to study radiation effects in advanced electronics will require greater cooperation and leverage amongst groups who share the same goals. In the short term, fiscal challenges will certainly be as significant if not more so than the technical challenges due to competing interests that want higher-performing systems with flat or reduced costs. Additional effort could be expended to study how different industrial base and government organizations could collaborate within the boundaries of existing regulations. The radiation community will band together, as it always has, and blaze a path that sits at the intersection of physics, materials science, and electrical engineering for the betterment of systems that serve national and international interests.

8 References

[1] *2011 International Technology Roadmap for Semiconductors*. Available: http://www.itrs.net/

[2] M. J. Gadlage, J. R. Ahlbin, B. Narasimham, B. L. Bhuva, L. W. Massengill, R. A. Reed, R. D. Schrimpf, and G. Vizkelethy, "Scaling Trends in SET Pulse Widths in Sub-100 nm Bulk CMOS Processes," *IEEE Trans. Nucl. Sci.*, vol. 57, no. 6, pp. 3336-3341, Dec. 2010.

[3] J. R. Ahlbin, M. J. Gadlage, D. R. Ball, A. W. Witulski, B. L. Bhuva, R. A. Reed, G. Vizkelethy, and L. W. Massengill, "The Effect of Layout Topology on Single-Event Transient Pulse Quenching in a 65 nm Bulk CMOS Process," *IEEE Trans. Nucl. Sci.*, vol. 57, no. 6, pp. 3380-3385, Dec. 2010.

[4] H. Park, *et al.*, "Laser-induced current transients in strained-Si diodes," *IEEE Trans. Nucl. Sci.*, vol. 56, no. 6, pp. 3203-3209, Dec. 2009.

[5] V. Ferlet-Cavrois, *et al.*, "A new technique for SET pulse width measurement in chains of inverters using pulsed laser irradiation," *IEEE Trans. Nucl. Sci.*, vol. 56, no. 4, pp. 2014-2020, Aug. 2009.

[6] J. A. Pellish, *et al.*, "Laser-induced current transients in silicon-germanium HBTs," *IEEE Trans. Nucl. Sci.*, vol. 55, no. 6, pp. 2936-2942, Dec. 2008.

[7] A. J. KleinOsowski, E. H. Cannon, J. A. Pellish, P. Oldiges, and L. Wissel, "Design Implications of Single Event Transients in a Commercial 45 nm SOI Device Technology," *IEEE Trans. Nucl. Sci.*, vol. 55, no. 6, pp. 3461-3466, Dec. 2008.

[8] M. J. Gadlage, *et al.*, "Assessing Alpha Particle-Induced Single Event Transient Vulnerability in a 90-nm CMOS Technology," *IEEE Electron Device Lett.*, vol. 29, no. 6, pp. 638-640, Jun. 2008.

[9] D. McMorrow, J. B. Boos, J. S. Melinger, V. Ferlet-Cavrois, P. Paillet, O. Duhamel, and J. Baggio, "Measurement of the transient response of semiconductor devices to ionizing radiation," *Nucl. Instr. and Meth. B*, vol. 261, no. 1-2, pp. 1137-1141, Aug. 2007.

[10] D. Kobayashi, H. Saito, and K. Hirose, "Estimation of single event transient voltage pulses in VLSI circuits from heavy-ion-induced transient currents measured in a single MOSFET," *IEEE Trans. Nucl. Sci.*, vol. 54, no. 4, pp. 1037-1041, Aug. 2007.

[11] D. Kobayashi, K. Hirose, T. Makino, H. Ikeda, and H. Saito, "Feasibility study of a table-based SET-pulse estimation in logic cells from heavy-ion-induced transient currents measured in a single MOSFET," *IEEE Trans. Nucl. Sci.*, vol. 54, no. 6, pp. 2347-2354, Dec. 2007.

[12] M. Gaillardin, P. Paillet, V. Ferlet-Cavrois, J. Baggio, D. McMorrow, O. Faynot, C. Jahan, L. Tosti, and S. Cristoloveanu, "Transient radiation response of single- and multiple-gate FD SOI transistors," *IEEE Trans. Nucl. Sci.*, vol. 54, no. 6, pp. 2355-2362, Dec. 2007.

[13] V. Ferlet-Cavrois, *et al.*, "New insights into single event transient propagation in chains of inverters - evidence for propagation-induced pulse broadening," *IEEE Trans. Nucl. Sci.*, vol. 54, no. 6, pp. 2338-2346, Dec. 2007.

[14] J. A. Pellish, *et al.*, "Heavy Ion Testing at the Galactic Cosmic Ray Energy Peak," presented at the 10th European Conference on Radiation and Its Effects on Components and Systems, Brugge, Belgium, 2009.

[15] K. M. Warren, *et al.*, "Application of RADSAFE to Model Single Event Upset Response of 0.25 μm CMOS SRAM," *IEEE Trans. Nucl. Sci.*, vol. 54, no. 4, pp. 898-903, Aug. 2007.

[16] R. A. Reed, *et al.*, "Impact of ion energy and species on single event effects analysis," *IEEE Trans. Nucl. Sci.*, vol. 54, no. 6, Dec. 2007.

[17] P. E. Dodd, *et al.*, "Impact of Heavy Ion Energy and Nuclear Interactions on Single-Event Upset and Latchup in Integrated Circuits," *IEEE Trans. Nucl. Sci.*, vol. 54, no. 6, pp. 2303-2311, 2007.

[18] R. A. Reed, R. A. Weller, R. D. Schrimpf, M. H. Mendenhall, K. M. Warren, and L. W. Massengill, "Implications of nuclear reactions for single event effects test methods and analysis," *IEEE Trans. Nucl. Sci.*, vol. 53, no. 6, pp. 3356-3362, Dec. 2006.

[19] K. P. Rodbell, *et al.*, "32 and 45 nm Radiation-Hardened-by-Design (RHBD) SOI Latches," *IEEE Trans. Nucl. Sci.*, vol. 58, no. 6, pp. 2702-2710, Dec. 2011.

[20] N. Seifert, B. Gill, J. A. Pellish, P. W. Marshall, and K. A. LaBel, "The Susceptibility of 45 and 32 nm Bulk CMOS Latches to Low-Energy Protons," *IEEE Trans. Nucl. Sci.*, vol. 58, no. 6, pp. 2711-2718, 2011.

[21] J. A. Pellish, *et al.*, "Impact of Spacecraft Shielding on Direct Ionization Soft Error Rates for Sub-130 nm Technologies," *IEEE Trans. Nucl. Sci.*, vol. 57, no. 6, pp. 3183-3189, Dec. 2010.

[22] B. D. Sierawski, *et al.*, "Impact of low-energy proton induced upsets on test methods and rate predictions," *IEEE Trans. Nucl. Sci.*, vol. 56, no. 6, pp. 3085-3092, Dec. 2009.

[23] D. F. Heidel, *et al.*, "Single-event upsets and multiple-bit upsets on a 45 nm SOI SRAM," *IEEE Trans. Nucl. Sci.*, vol. 56, no. 6, pp. 3499-3504, Dec. 2009.

[24] G. R. Hopkinson, C. J. Dale, and P. W. Marshall, "Proton effects in charge-coupled devices," *IEEE Trans. Nucl. Sci.*, vol. 43, no. 2, pp. 614-627, 1996.

[25] J. C. Pickel, A. H. Kalma, G. R. Hopkinson, and C. J. Marshall, "Radiation effects on photonic imagers-a historical perspective," *IEEE Trans. Nucl. Sci.*, vol. 50, no. 3, pp. 671-688, 2003.

[26] J. R. Srour, C. J. Marshall, and P. W. Marshall, "Review of displacement damage effects in silicon devices," *IEEE Trans. Nucl. Sci.*, vol. 50, no. 3, pp. 653-670, 2003.

[27] D. B. Strukov, G. S. Snider, D. R. Stewart, and R. S. Williams, "The missing memristor found," *Nature*, vol. 453, no. 7191, pp. 80-83, 2008.

[28] D. Manners. (2011). *IEF2011: HP to replace flash and SSD in 2013*. Available: http://www.electronicsweekly.com/Articles/06/10/2011/51988/ief2011-hp-to-replace-flash-and-ssd-in-2013.htm

[29] P. Taylor. (2012). *DDR4 makes it debut at ISSCC 2012*. Available: http://news.techeye.net/chips/ddr4-makes-its-debut-at-isscc-2012

[30] (2012). *Elpida seeks bankruptcy protection*. Available: http://www.japantimes.co.jp/text/nb20120228n1.html

[31] R. Pease, "Microelectronic Piece Part Radiation Hardness Assurance for Space Systems," presented at the Nuclear and Space Radiation Effects Conf. Short Course, *IEEE*: Atlanta, GA, 2004.

[32] K. Kohnen and K. Jobe, "Selection of Integrated Circuits for Space Systems: Electronic Designer's Perspective," presented at the Nuclear and Space Radiation Effects Conf. Short Course, *IEEE*: Quebec City, 2009.

[33] "Transistors go 3-D," *Spectrum, IEEE*, vol. 48, no. 6, pp. 12-12, 2011.

[34] P. W. Marshall, M. A. Carts, A. Campbell, D. McMorrow, S. Buchner, R. Stewart, B. Randall, B. Gilbert, and R. A. Reed, "Single event effects in circuit-hardened SiGe HBT logic at gigabit per second data rates," *IEEE Trans. Nucl. Sci.*, vol. 47, no. 6, pp. 2669-2674, Dec. 2000.

[35] J. D. Cressler and G. Niu, *Silicon-germanium heterojunction bipolar transistors*. Boston, MA: Artech House, 2003.

[36] J. D. Cressler, "On the potential of SiGe HBTs for extreme environment electronics," *Proc. IEEE*, vol. 93, no. 9, pp. 1559-1582, Sep. 2005.

[37] P. W. Marshall, *et al.*, "Autonomous Bit Error Rate Testing at Multi-Gbit/s Rates Implemented in a 5AM SiGe Circuit for Radiation Effects Self Test (CREST)," *IEEE Trans. Nucl. Sci.*, vol. 52, no. 6, pp. 2446-2454, Dec. 2005.

[38] R. A. Reed, *et al.*, "Heavy-ion broad-beam and microprobe studies of single-event upsets in 0.21 μm SiGe heterojunction bipolar transistors and circuits," *IEEE Trans. Nucl. Sci.*, vol. 50, no. 6, pp. 2184-2190, Dec. 2003.

[39] J. D. Cressler, Ed., *Silicon heterostructure handbook : materials, fabrication, devices, circuits, and applications of SiGe and Si strained-layer epitaxy*. Boca Raton, FL: CRC Taylor & Francis, 2006, 1248 pages.

[40] J. A. Pellish, *et al.*, "A generalized SiGe HBT single-event effects model for on-orbit event rate calculations," *IEEE Trans. Nucl. Sci.*, vol. 54, no. 6, pp. 2322-2329, Dec. 2007.

[41] J. L. Barth, "Modeling Space Radiation Environments," presented at the Nuclear and Space Radiation Effects Short Course, *IEEE*: Snowmass Village, CO, 1997.

[42] M. A. Xapsos, "Modeling the space radiation environment," presented at the Nuclear and Space Radiation Effects Conf. Short Course, *IEEE*: Ponte Vedra Beach, FL, 2006.

[43] J. L. Barth, "Evolution of the Radiation Environments," presented at the European Conf. on Radiation and Its Effects on Components and Systems Short Course, Bruges, Belgium, 2009.

[44] J. Feynman, G. Spitale, J. Wang, and S. Gabriel, "Interplanetary Proton Fluence Model: JPL 1991," *J. Geophys. Res.*, vol. 98, no. A8, pp. 13281-13294, 1993.

[45] G. Badhwar and P. M. O'Neill, "Galactic cosmic radiation model and its applications," *Adv. Space. Res.*, vol. 17, no. 2, pp. 7-17, 1996.

[46] R. A. Mewaldt, "Galactic Cosmic-Ray Composition and Energy-Spectra," *Adv. Space Res.,* vol. 14, no. 10, pp. 737-747, 1994.

[47] R. A. Nymmik, M. I. Panasyuk, T. I. Pervaja, and A. A. Suslov, "A model of galactic cosmic ray fluxes," *Nucl. Tracks Radiat. Meas.*, vol. 20, no. 3, pp. 427-429, 1992.

[48] A. J. Tylka, *et al.*, "CREME96: a revision of the Cosmic Ray Effects on Micro-Electronics Code," *IEEE Trans. Nucl. Sci.,* vol. 44, no. 6, pp. 2150-2160, Dec. 1997.

[49] R. A. Nymmik, M. I. Panasyuk, and A. A. Suslov, "Galactic cosmic ray flux simulation and prediction," *Adv. Space Res.,* vol. 17, no. 2, pp. 19-30, 1996.

[50] G. D. Badhwar, P. M. O'Neill, and A. G. Troung, "Galactic cosmic radiation environment models," in *Space Technology and Applications International Forum-2001*. vol. 552, M. S. ElGenk, Ed., ed Melville: Amer Inst Physics, 2001, pp. 1179-1184.

[51] J. W. Wilson, F. A. Cucinotta, J. L. Shinn, L. C. Simonsen, R. R. Dubey, W. R. Jordan, T. D. Jones, C. K. Chang, and M. Y. Kim, "Shielding from solar particle event exposures in deep space," *Radiation Measurements,* vol. 30, no. 3, pp. 361-382, Jun 1999.

[52] D. Reames, "Particle acceleration at the Sun and in the heliosphere," *Space Science Reviews,* vol. 90, no. 3, pp. 413-491, 1999.

[53] M. H. Y. Kim, F. A. Cucinotta, and J. W. Wilson, "Mean occurrence frequency and temporal risk analysis of solar particle events," *Radiation Measurements,* vol. 41, no. 9-10, pp. 1115-1122, Oct-Nov 2006.

[54] M. A. Xapsos, G. P. Summers, J. L. Barth, E. G. Stassinopoulos, and E. A. Burke, "Probability model for worst case solar proton event fluences," *Nuclear Science, IEEE Transactions on,* vol. 46, no. 6, pp. 1481-1485, 1999.

[55] M. A. Xapsos, G. P. Summers, J. L. Barth, E. G. Stassinopoulos, and E. A. Burke, "Probability model for cumulative solar proton event fluences," *IEEE Trans. Nucl. Sci.,* vol. 47, no. 3, pp. 486-490, Jun. 2000.

[56] E. T. Jaynes, "Information Theory and Statistical Mechanics," *Phys. Rev.,* vol. 106, no. 4, pp. 620-630, 1957.

[57] M. A. Xapsos, C. Stauffer, T. Jordan, J. L. Barth, and R. A. Mewaldt, "Model for cumulative solar heavy ion energy and linear energy transfer spectra," *IEEE Trans. Nucl. Sci.,* vol. 54, no. 6, pp. 1985-1989, Dec. 2007.

[58] W. N. Spjeldvik and P. L. Rothwell, "The earth‘s radiation belts," Air Force Geophysics Laboratory, Hanscomb AFB, Rep. AFGL-TR-83-0240, 1983.

[59] E. G. Stassinopoulos and J. P. Raymond, "The Space Radiation Environment for Electronics," *Proc. IEEE,* vol. 76, no. 11, pp. 1423-1442, Nov 1988.

[60] E. J. Daly, J. Lemaire, D. Heynderickx, and D. J. Rodgers, "Problems with models of the radiation belts," *IEEE Trans. Nucl. Sci.,* vol. 43, no. 2, pp. 403-415, 1996.

[61] C. E. McIlwain, "Coordinates for Mapping Distribution of Magnetically Trapped Particles," *J. Geophys. Res.,* vol. 66, no. 11, pp. 3681-3691, 1961.

[62] K. A. LaBel, S. Way, E. G. Stassinopoulos, C. M. Crabtree, J. Hengemihle, and M. M. Gates, "Solid State Tape Recorders: Spaceflight SEU Data For SAMPEX And

TOMS/Meteor-3," in *IEEE Radiation Effects Data Workshop*, Snowbird, UT, 1993, pp. 77-84.

[63] J. L. Barth, J. W. Adolphsen, and G. B. Gee, "Single event effects on commercial SRAMs and power MOSFETs: final results of the CRUX flight experiment on APEX," in *IEEE Radiation Effects Data Workshop*, Newport Beach, CA, 1998, pp. 1-10.

[64] D. M. Sawyer and J. I. Vette, "Trapped Particle Environment for Solar Maximum and Solar Minimum (AP8)," NSSDC Report 76-06, 1976.

[65] J. D. Meffert and M. S. Gussenhoven, "CRRESPRO Documentation," Phillips Laboratory, PL-TR-94-2218, 1994.

[66] D. Heynderickx, M. Kruglanski, V. Pierrard, J. Lemaire, M. D. Looper, and J. B. Blake, "A low altitude trapped proton model for solar minimum conditions based on SAMPEX/PET data," *IEEE Trans. Nucl. Sci.*, vol. 46, no. 6, pp. 1475-1480, 1999.

[67] H. B. Garrett and I. Jun, "Spacecraft Environment Interactions," presented at the Nuclear and Space Radiation Effects Conf. Short Course, *IEEE*: Las Vegas, NV, 2011.

[68] J. I. Vette, "The AE-8 Trapped Electron Model Environment," Rep. NSSDC/WDC-A-R&S 91-24, 1991.

[69] D. H. Brautigam and J. T. Bell, "CRRESELE Documentation," Phillips Laboratory, PL-TR-95-2128, 1995.

[70] D. M. Boscher, S. A. Bourdarie, R. H. W. Friedel, and R. D. Belian, "Model for the geostationary electron environment: POLE," *IEEE Trans. Nucl. Sci.*, vol. 50, no. 6, pp. 2278-2283, Dec 2003.

[71] A. S. Piet, S. Bourdarie, D. Boscher, and R. H. W. Friedel, "A Model for the Geostationary Electron Environment: POLE, From 30 keV to 5.2 MeV," *IEEE Trans. Nucl. Sci.*, vol. 53, no. 4, pp. 1844-1850, Aug 2006.

[72] A. Sicard-Piet, S. Bourdarie, D. Boscher, R. H. W. Friedel, M. Thomsen, T. Goka, H. Matsumoto, and H. Koshiishi, "A new international geostationary electron model: IGE-2006, from 1 keV to 5.2 MeV," *Space Weather*, vol. 6, no. 7, p. S07003, 2008.

[73] J. R. Wertz, D. F. Everett, and J. J. Puschell, Eds., *Space Mission Engineering: The New SMAD*. Microcosm Press, 2011, 1048 pages.

[74] G. Santin, D. Wright, and M. Asai, "Space Radiation Transport Models," in *Nuclear and Space Radiation Effects Conf. Short Course*, Ponte Vedra Beach, FL, 2006.

[75] R. Reed, "Fundamental Mechanisms for Single Particle-Induced Soft Errors," in *Nuclear and Space Radiation Effects Conf. Short Course*, Tucson, AZ, 2008.

[76] J. F. Zeigler, "SRIM-2003," *Nucl. Instr. and Meth. B*, vol. 219-220, pp. 1027-1036, Jun. 2004.

[77] E. L. Petersen, *Single Event Effects in Aerospace*. Hoboken, NJ: IEEE Press, 2011.

[78] W. Heinrich, "Calculation of LET Spectra of Heavy Cosmic Ray Nuclei at Various Absorber Depths," *Radiat. Eff. Defects Solids*, vol. 34, no. 1-3, pp. 143-148, 1977.

[79] R. D. Evans, *The atomic nucleus*. New York,: McGraw-Hill, 1955.

[80] F. B. McLean and T. R. Oldham, "Basic Mechanisms of Radiation Effects in Electronic Materials and Devices," Harry Diamond Labs, Technical Report HDL-TR-2129, 1987.

[81] T. R. Oldham and F. B. McLean, "Total ionizing dose effects in MOS oxides and devices," *Nuclear Science, IEEE Transactions on*, vol. 50, no. 3, pp. 483-499, 2003.

[82] R. C. Hughes, "Charge-Carrier Transport Phenomena in Amorphous SiO2: Direct Measurement of the Drift Mobility and Lifetime," *Phys. Rev. Lett.*, vol. 30, no. 26, pp. 1333-1336, 1973.

[83] R. L. Pease, "Total ionizing dose effects in bipolar devices and circuits," *IEEE Trans. Nucl. Sci.*, vol. 50, no. 3, pp. 539-551, 2003.

[84] E. W. Enlow, R. L. Pease, W. Combs, R. D. Schrimpf, and R. N. Nowlin, "Response of advanced bipolar processes to ionizing radiation," *IEEE Trans. Nucl. Sci.*, vol. 38, no. 6, pp. 1342-1351, Dec. 1991.

[85] R. Baumann, "Single-Event Effects in Advanced CMOS Technology," in *Nuclear and Space Radiation Effects Conf. Short Course*, Seattle, WA, 2005.

[86] S. Buchner, "Overview of Single Event Effects," presented at the Int. School on the Effects of Radiation on Embedded Systems for Space Applications, Toulouse, France, 2011.

[87] M. R. Shaneyfelt, J. R. Schwank, P. E. Dodd, and J. A. Felix, "Total Ionizing Dose and Single Event Effects Hardness Assurance Qualification Issues for Microelectronics," *IEEE Trans. Nucl. Sci.*, vol. 55, no. 4, pp. 1926-1946, Aug. 2008.

[88] M. R. Shaneyfelt, J. R. Schwank, S. C. Witczak, D. M. Fleetwood, R. L. Pease, P. S. Winokur, L. C. Riewe, and G. L. Hash, "Thermal-stress effects and enhanced low dose rate sensitivity in linear bipolar ICs," *IEEE Trans. Nucl. Sci.*, vol. 47, no. 6, pp. 2539-2545, Dec. 2000.

[89] R. Ladbury, "Combined Effects on DDR Class Memories," presented at the NEPP Electronic Technology Workshop, Greenbelt, MD, 2011.

[90] J. Krieg, *et al.*, "Hardness assurance implications of bimodal total dose response in a bipolar linear voltage comparator," *IEEE Trans. Nucl. Sci.*, vol. 46, no. 6, pp. 1627-1632, Dec. 1999.

[91] R. Ladbury and J. L. Gorelick, "Statistical methods for large flight lots and ultra-high reliability applications," *IEEE Trans. Nucl. Sci.*, vol. 52, no. 6, pp. 2630-2637, Dec. 2005.

[92] R. Ladbury and B. Triggs, "A Bayesian Approach for Total Ionizing Dose Hardness Assurance," *IEEE Trans. Nucl. Sci.*, vol. 58, no. 6, pp. 3004-3010, Dec. 2011.

[93] R. Ladbury, J. L. Gorelick, M. A. Xapsos, T. O'Connor, and S. Demosthenes, "A Bayesian treatment of risk for radiation hardness assurance," in *8th European Conference on Radiation and Its Effects on Components and Systems*, Cap d'Agde, France, 2005, pp. PB1-1-PB1-8.

[94] R. A. Weller, A. L. Sternberg, L. W. Massengill, R. D. Schrimpf, and D. M. Fleetwood, "Evaluating average and atypical response in radiation effects simulations," *IEEE Trans. Nucl. Sci.*, vol. 50, no. 6, pp. 2265-2271, Dec. 2003.

[95] R. A. Weller, M. H. Mendenhall, R. A. Reed, R. D. Schrimpf, K. M. Warren, B. D. Sierawski, and L. W. Massengill, "Monte Carlo Simulation of Single Event Effects," *IEEE Trans. Nucl. Sci.*, vol. 57, no. 4, pp. 1726-1746, Aug. 2010.

[96] M. P. King, R. A. Reed, R. A. Weller, M. H. Mendenhall, R. D. Schrimpf, M. L. Alles, E. C. Auden, S. E. Armstrong, and M. Asai, "The Impact of Delta-Rays on Single-Event Upsets in Highly Scaled SOI SRAMs," *IEEE Trans. Nucl. Sci.*, vol. 57, no. 6, pp. 3169-3175, Dec. 2010.

[97] K. M. Warren, *et al.*, "Monte-Carlo based on-orbit single event upset rate prediction for a radiation hardened by design latch," *IEEE Trans. Nucl. Sci.*, vol. 54, no. 6, pp. 2419-2425, Dec. 2007.

[98] A. D. Tipton, *et al.*, "Device-Orientation Effects on Multiple-Bit Upset in 65 nm SRAMs," *IEEE Trans. Nucl. Sci.*, vol. 55, no. 6, pp. 2880-2885, Dec. 2008.

[99] D. G. Mavis, P. H. Eaton, and M. D. Sibley, "SEE characterization and mitigation in ultra-deep submicron technologies," in *2009 Int. Conf. on IC Design and Technology*, Austin, TX, 2009, pp. 105-112.

[100] J. M. Hutson, *et al.*, "Evidence for Lateral Angle Effect on Single-Event Latchup in 65 nm SRAMs," *IEEE Trans. Nucl. Sci.*, vol. 56, no. 1, pp. 208-213, Feb. 2009.

[101] K. P. Rodbell, D. F. Heidel, H. H. K. Tang, M. S. Gordon, P. Oldiges, and C. E. Murray, "Low-Energy Proton-Induced Single-Event-Upsets in 65 nm node, Silicon-on-Insulator, Latches and Memory Cells," vol. 54, no. 6, pp. 2474-2479, Dec. 2007.

[102] D. F. Heidel, *et al.*, "Low energy proton single-event upset test results on 65 nm SOI SRAM," *IEEE Trans. Nucl. Sci.*, vol. 55, no. 6, pp. 3394-3400, Dec. 2008.

[103] J. A. Pellish, *et al.*, "Low-Energy Proton Testing Using Cyclotron Sources," presented at the Nuclear and Space Radiation Effects Conf., Las Vegas, NV, 2011.

[104] B. D. Sierawski, *et al.*, "Muon-Induced Single Event Upsets in Deep-Submicron Technology," *IEEE Trans. Nucl. Sci.*, vol. 57, no. 6, pp. 3273-3278, Dec. 2010.

[105] B. D. Sierawski, R. A. Reed, M. H. Mendenhall, R. A. Weller, R. D. Schrimpf, S.-J. Wen, R. Wong, N. Tam, and R. C. Baumann, "Effects of scaling on muon-induced soft errors," in *2011 Int. Reliability Physics Symp.*, 2011, pp. 3C.3.1-3C.3.6.

[106] R. Ladbury, M. D. Berg, K. A. LaBel, M. Friendlich, A. Phan, and H. Kim, "Radiation Performance of 1 Gbit DDR2 SDRAMs Fabricated with 80-90 nm CMOS," in *IEEE Radiation Effects Data Workshop*, Tucson, AZ, 2008, pp. 42-46.

[107] J. M. Hutson, J. A. Pellish, G. Boselli, R. Baumann, R. A. Reed, R. D. Schrimpf, R. A. Weller, and L. W. Massengill, "The Effects of Angle of Incidence and Temperature on Latchup in 65 nm Technology," *IEEE Trans. Nucl. Sci.*, vol. 54, no. 6, pp. 2541-2546, Dec. 2007.

[108] H. Paul. (2012). *Stopping Power for Light Ions: Graphs, Data, Comments and Programs*. Available: http://www.exphys.jku.at/stopping/

[109] E. H. Cannon, M. Cabanas-Holmen, J. Wert, T. Amort, R. Brees, J. Koehn, B. Meaker, and E. Normand, "Heavy Ion, High-Energy, and Low-Energy Proton SEE Sensitivity of 90-nm RHBD SRAMs," *IEEE Trans. Nucl. Sci.,* vol. 57, no. 6, pp. 3493-3499, Dec. 2010.

[110] N. Haddad, A. Kelly, R. Lawrence, B. Li, J. Rodgers, and J. Ross, "Heavy ion, high energy and low energy proton SEE sensitivity of 90-nm RHBD SRAMs," presented at the European Conf. on Radiation and Its Effects on Components and Systems, Langenfeld, Austria, 2010.

[111] H. Paul and A. Schinner, "An empirical approach to the stopping power of solids and gases for ions from 3Li to 18Ar," *Nuc. Instr. and Meth. B,* vol. 179, no. 3, pp. 299-315, 2001.

[112] H. Paul and A. Schinner, "An empirical approach to the stopping power of solids and gases for ions from 3Li to 18Ar – Part II," *Nuc. Instr. and Meth. B,* vol. 195, no. 1–2, pp. 166-174, 2002.

[113] H. Paul and A. Schinner, "Judging the reliability of stopping power tables and programs for protons and alpha particles using statistical methods," *Nucl. Instr. and Meth. B,* vol. 227, no. 4, pp. 461-470, 2005.

[114] M. Pavlovič and I. Strašík, "Supporting routines for the SRIM code," *Nucl. Instr. and Meth. B,* vol. 257, no. 1-2, pp. 601-604, Apr. 2007.

[115] I. Strašík and M. Pavlovič, "Improvements to the SRIM simulations," *Radiation Effects and Defects in Solids,* vol. 164, no. 7-8, pp. 470-476, Aug. 2009.

[116] J. F. Zeigler and J. P. Biersack. (2011). *Stopping and Range of Ions in Matter*. Available: http://www.srim.org/

[117] "Stopping Powers and Ranges for Protons and Alph Particles," ICRU Report 49, 1993.

[118] S. Agostinelli, *et al.*, "Geant4—a simulation toolkit," *Nucl. Instr. and Meth. A,* vol. 506, no. 3, pp. 250-303, 2003.

[119] J. Allison, *et al.*, "Geant4 developments and applications," *IEEE Trans. Nucl. Sci.,* vol. 53, no. 1, pp. 270-278, Feb. 2006.

[120] R. A. Reed, J. Kinnison, J. C. Pickel, S. Buchner, P. W. Marshall, S. Kniffin, and K. A. LaBel, "Single-event effects ground testing and on-orbit rate prediction methods: the past, present, and future," *IEEE Trans. Nucl. Sci.,* vol. 50, no. 3, pp. 622-634, Jun. 2003.

[121] R. A. Weller, R. A. Reed, K. M. Warren, M. H. Mendenhall, B. D. Sierawski, R. D. Schrimpf, and L. W. Massengill, "General framework for single event effects rate prediction in microelectronics," *IEEE Trans. Nucl. Sci.,* vol. 56, no. 6, pp. 3098-3108, Dec. 2009.

[122] P. Calvel, C. Barillot, A. Porte, G. Auriel, C. Chatry, P. F. Peyrard, G. Santin, R. Ecoffet, and T. M. Jordan, "Review of Deposited Dose Calculation Methods Using Ray Tracing Approximations," *IEEE Trans. Nucl. Sci.,* vol. 55, no. 6, pp. 3106-3113, Dec. 2008.

[123] T. M. Jordan, "An adjoint charged particle transport method," *IEEE Trans. Nucl. Sci.,* vol. 23, no. 6, pp. 1857-1861, Dec. 1976.

[124] T. M. Jordan, "Space system analysis using the NOVICE code system," in *Radiation and its Effects on Devices and Systems, 1991. RADECS 91., First European Conference on*, 1991, pp. 312-316.